Section 1

Atmospheric data assimilation schemes, analysis and initialization, data impact studies, observing system experiments

Evolution of Météo-France global ensemble data assimilation and high resolution regional experimentation of ensemble assimilation

Loïk Berre, Pierre Brousseau, Laure Raynaud, Gérald Desroziers, Carole Labadie, Laurent Descamps, Météo-France/CNRS, CNRM/GAME

Since July 2008, a global variational ensemble assimilation system is run operationally at Météo-France with the ARPEGE system. This enables flow-dependent forecast error variances to be produced for the data assimilation system. This ensemble assimilation system is also used to initialize operational ensemble forecasts. However, the evolution of ensemble perturbations relies currently on a perfect model assumption, and resulting error variances are increased a posteriori, to account for contribution of model error to variances.
Studies are being conducted to estimate and represent model error contributions to the perturbation evolution more accurately. Departures between forecasts and observations, which provide total forecast error estimates (sum of evolved initial uncertainties and of model errors), are compared to the evolved ensemble assimilation spread (corresponding to forecast errors due to initial uncertainties). This comparison allows model error variances to be estimated objectively. This information is then used to amplify perturbations after each forecast step (by 10% approximately, every six hours). Compared to the spread obtained when using a perfect model assumption, this inflation technique allows the ensemble spread to be increased by a factor 2.
The effective amplification of perturbations is particularly pronounced in low pressure systems (see Figure 1). Moreover, new variance estimates have a positive impact on the forecast quality, in addition of being more consistent with observation-based estimates. This model error representation in the ensemble assimilation system appears to be also beneficial for the ensemble prediction system, due to the increased realism of ensemble spread in particular. It is thus considered to implement this approach operationally in the near future.

Another important area of ongoing research at Météo-France is the experimentation of ensemble variational assimilation with the high resolution regional model AROME (with a 2.5 km resolution). In the operational version of AROME-France, the flow dependence of background error covariances is currently neglected. In order to relax this static approach, geographically averaged covariances can be calculated daily using an AROME ensemble assimilation, which is coupled to the operational ARPEGE ensemble assimilation based on the same principles.
These statistics depend on the meteorological phenomena encountered. Background error variances are smaller in anticyclonic situations, excepted for temperature and humidity in low troposphere, where the uncertainty due to the fog and low cloud events remains important. In convective situations these variances are larger, representing the uncertainty associated to convective phenomena. Spatial correlation differences are illustrated by single observation experiments (Figure 2) : the analysis increment caused by a given departure between observation and background is more (resp. less) extended horizontally (resp. vertically) in an anticyclonic situation than in a convective one. Under the observation location, the impact on the wind field is also different : the cooling increment has a weak influence in the first case, whereas it generates a strong divergent circulation in the second one.
Studies have shown a positive impact of these covariances of the day on the data assimilation system behaviour and on the forecast quality. These results support the idea to implement an AROME ensemble variational assimilation system operationally.

(a)

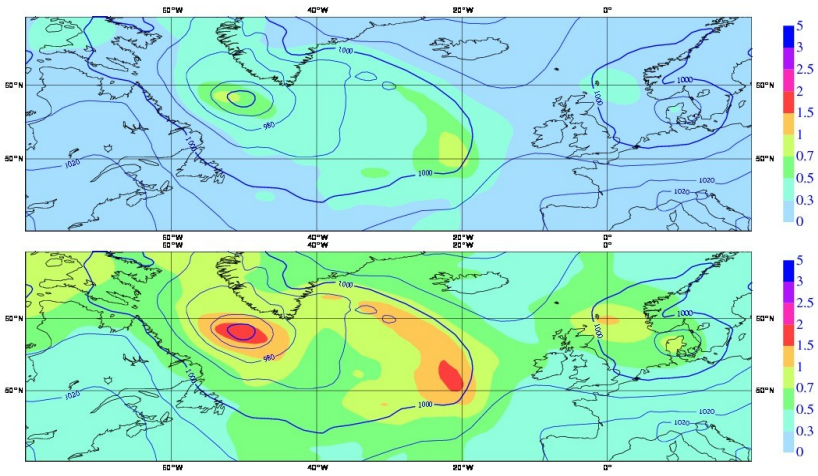

Figure 1 : Amplitude of forecast perturbations for surface pressure (iso-colors, in hPa), derived from the ARPEGE ensemble assimilation system. Top : based on a perfect model assumption. Bottom : including a model error representation in the evolution of perturbations. The mean sea level pressure field is overlaid with blue isolines (iso-contours : 10 hPa).

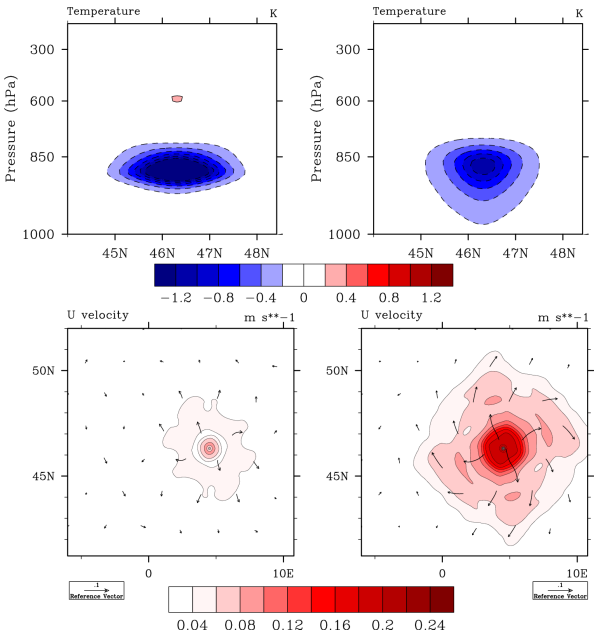

Figure 2 : AROME analysis increment (difference between analysis and background) caused by a given innovation (difference between observation and background) of temperature at 850 hPa using background error covariances calculated for an anticyclonic (left) and a convective (right) situation : vertical cross section of temperature increment (top) and horizontal cross section at 950 hPa of wind increment (bottom).

Assimilation of Synthetic Aperture Radar (SAR) wind information in Environment Canada's limited-area analysis system

Rick Danielson (@ec.gc.ca), Luc Fillion, and Harold Ritchie
Meteorological Research Division (Dorval), Environment Canada

Introduction

New observational platforms can be challenging to incorporate into a weather forecast system. In part, this is because there is simply more data to assimilate and their weighting may be unclear, but observed scales and physical processes may not be fully resolved as well. Such is the case for satellite SARs that provide O[1-km] ocean wind, current (Chapron et al. 2005), and possibly wave breaking information (Hwang et al. 2010). A simplification (as in previous work) is to interpret SAR backscatter following established methods of scatterometer wind retrieval. Although we are motivated by the assimilation of such retrievals, we believe a more natural treatment of SAR observations follows an approach that is both direct (i.e., that assimilates backscatter instead of derived wind) and inclusive of smaller scales (i.e., that benefits from scales unresolved by more conventional observing platforms). The ongoing development of high resolution data assimilation methods facilitates an exploration of this approach.

Two analysis configurations

Fillion et al. (2010) introduce hemispheric (HEM) and bi-Fourier (BF) approaches to incremental 3-D variational analysis in the Global Environmental Multiscale (GEM) forecast system. Both approaches employ background error correlations that are horizontally homogeneous and isotropic for all wavenumbers, with non-separable vertical and horizontal structures. Error statistics are derived using lagged forecast differences (the so-called NMC method). Dynamical balance is dictated by the spectral cross-correlations, although these appear to be negligible at smaller scales (not shown). We choose to assimilate only observations within the smaller 15-km BF analysis domain (Fig.1a), even for the larger 55-km HEM domain (not shown), so that analysis impacts can be compared. Perhaps as expected, the wavelength of the response (in terms of analysis increments following SAR assimilation) tends to be shorter in our experimental BF configuration (Fig.1c) than in the operational HEM configuration (Fig.1b).

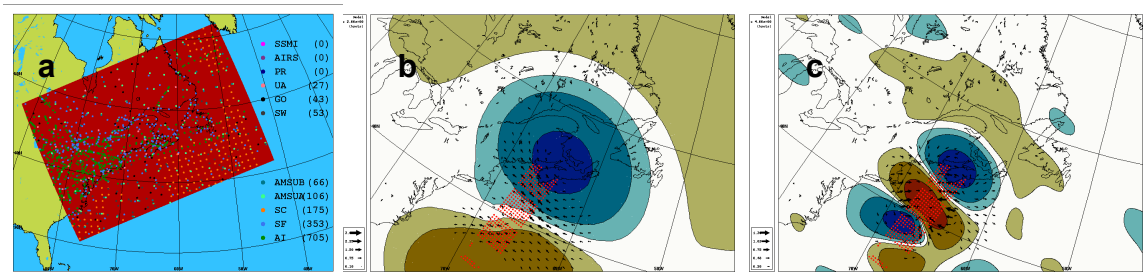

Fig. 2: A typical 6-h subset of observations (dots) within the BF analysis domain (red) from a) conventional platforms and b,c) Radarsat-2 SAR, with b) HEM and c) BF analysis increments of surface wind and temperature following SAR assimilation (note: temperature contour interval in b) is larger than in c)).

Assimilation experiments

Short-term GEM simulations at 15-km resolution were performed for 60 assimilation periods (centered at 00/12 UTC) between 10 Nov and 20 Dec 2009. These provided background trajectories for the assimilation of conventional observations and 209 east coast Radarsat-2 scenes (acquired around 10/22 UTC). Innovations (observation minus GEM background) were calculated relative to the appropriate time within these GEM 6-h trajectories. Buoy wind observations from 46 platforms were not assimilated so that SAR errors could first be postulated and the resulting analyses then validated. The HEM approach was found to be more sensitive to SAR wind information than our BF approach. The largest HEM analysis-buoy differences were obtained when conventional observations were assimilated alone (cf. Fig. 2c). Differences were reduced if SAR was included, but no assimilation (cf. Fig. 2a) seemed better. The smallest analysis-buoy differences were obtained for SAR-only assimilation (cf. Fig. 2d).

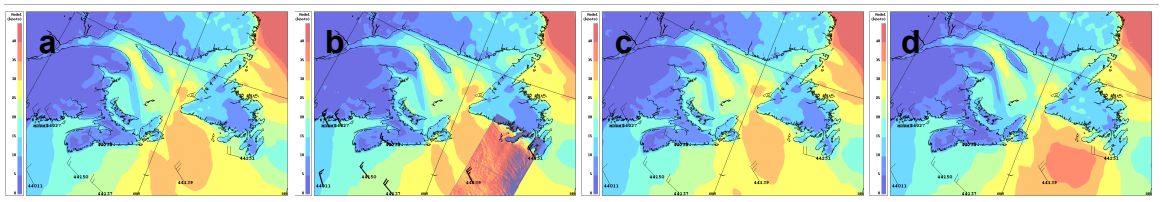

Fig. 2: Surface wind speed from a) a GEM forecast, b) direct SAR retrieval using GEM wind direction, and assimilation of c) conventional observations, and d) SAR backscatter

Conclusions

A new framework now exists for testing the impact SAR assimilation, perhaps for the first time, in a quasi-operational setting. Environment Canada's unified variational code has been employed to define a high resolution GEM error covariance matrix for bi-Fourier limited-area analysis (an approach not yet fully exploited). SAR assimilation may already be beneficial using a hemispheric assimilation scheme that has recently become operational. Once this impact can be confirmed to compare favourably with that of more conventional observation platforms, a formal assessment of short term forecasts may be undertaken.

References and acknowledgements

Chapron, B., F. Collard, and F. Ardhuin, 2005: Direct measurements of ocean surface velocity from space: Interpretation and validation, *J. Geophys. Res.*, **110,** C07008, doi:10.1029/2004JC002809.

Danielson R. E., M. Dowd, and H. Ritchie, 2008: Objective analysis of marine winds with the benefit of the Radarsat-1 synthetic aperture radar: A nonlinear regression framework, *J. Geophys. Res.,* **113,** C05019, doi:10.1029/2007JC004413.

Fillion, L., M. Tanguay, E. Lapalme, B. Denis, M. Desgagne, V. Lee, N. Ek, Z. Liu, M. Lajoie, J.-F. Caron, and C. Pagé, 2010: The Canadian regional data assimilation and forecasting system. *Wea. Forecasting,* **25,** pp. 1645-1669.

Hwang, P. A., B. Zhang, and W. Perrie, 2010: Depolarized radar return for breaking wave measurement and hurricane wind retrieval, *Geophys. Res. Lett.,* **37,** L01604, doi:10.1029/2009GL041780.

This work is being funded by the Canadian Space Agency. SAR data was taken from archives of the Canadian Centre for Remote Sensing.

Development of JMA Local Analysis

Junya Fukuda, Tadashi Fujita, Yasutaka Ikuta,
Yoshihiro Ishikawa and Koichi Yoshimoto
Numerical Prediction Division, Japan Meteorological Agency
1-3-4 Otemachi, Chiyoda-ku, Tokyo 100-8122, Japan
E-mail: jfukuda@met.kishou.go.jp, t-fujita@met.kishou.go.jp

1. Introduction

The Japan Meteorological Agency (JMA) is developing the Local NWP system – a high-resolution numerical weather prediction system aimed at supporting aviation and disaster-prevention information services. It consists of a forecast model called the Local Forecast Model (LFM) with a horizontal grid spacing of 2 km and an objective analysis called Local Analysis (LA) that prepares the initial condition for the LFM. The LA and LFM domains are shown in Fig. 1. JMA has been conducting trial operation of the Local NWP system since November 2010, and will start actual operation in 2012 after the introduction of a new supercomputer.

2. Design of the Local Analysis system

LA was constructed using JNoVA-3Dvar – a three-dimensional variational data assimilation system based on JMA's non-hydrostatic model (JMA-NHM; Saito et al. 2006). JNoVA-3DVar is a degenerate version of JNoVA-4DVar (Honda et al. 2005). In order to frequently update analysis reflecting information from new observation data within a short time while minimizing the usage of computer resources, a rapid update cycle method is employed in which JNoVA-3DVar and one-hour forecasts of the JMA-NHM are executed in turn (Fig. 2). In addition to the observations listed in Ishimizu and Ujiie (2010), data on total column water vapor from the ground-based GPS (Ishikawa 2010) have been used since August 2010. At the same time, the number of Doppler radar sites used in the assimilation has been increased from 10 to 18, thereby improving the coverage of radial velocity observation. Quality control for surface station data has been introduced to take into account the representativeness error estimated based on statistics of difference and the correlation between observation and model forecasts since September 2010.

3. Recent developments

i) Vertical coordinate system of control variables

In the current system, 3DVar control variables are defined in z*-coordinate system. With this vertical coordinate system, the influence of topography on the analysis increment remains strong up to high altitudes (Fig. 3 (a)). In order to remedy this problem, we tried a new vertical coordinate system based on one by Ishida (2007) designed to follow terrain near the surface and rapidly shift to z-coordinate system higher up. Figure 3 (b) shows that the new coordinate system reasonably limits the influence of topography on the analysis increment in the lower troposphere.

ii) Surface observation operator

Observations from surface stations are assimilated in LA. The observation operator of JNoVA-3DVar diagnoses surface temperature based on similarity theory, and refers to potential temperatures at ground level and at the lowest atmospheric model level. Implementation of an update is under way to extend the 3DVar control variable to include potential temperature at ground level in addition to the variables on the atmospheric model levels. This update is found to mitigate excessive temperature increment in the lower troposphere. Using the analyzed potential temperature at the ground level to start the following forecast in the rapid update cycle helps to keep the lower boundary condition of the atmosphere consistent with analysis of the lower troposphere. The example shown in Fig. 4 indicates that assimilating surface temperature observations along with total column water vapor observations from the ground-based GPS assists the LFM in forecasting precipitation related to heated land in the afternoon.

4. Summary

Various efforts are being made to improve LA toward the planned operational use of the system in 2012. A new vertical coordinate system is being tested to control the effects of terrain on analysis increments, and the surface observation operator is being revised to secure more reasonable analysis in the lower troposphere. Further developments to improve LA are also under

way, including assimilation of relative humidity data retrieved from radar reflectivity observation (Ikuta and Honda 2011).

References

Honda, Y., M. Nishijima, K. Koizumi, Y. Ohta, K. Tamiya, T. Kawabata and T. Tsuyuki, 2005: A pre-operational variational data assimilation system for a non-hydrostatic model at the Japan Meteorological Agency: Formulation and preliminary results. *Q. J. R. Meteorol. Soc.*, **131**, 3465 – 3475.

Ikuta, Y., and Y. Honda, 2011: Development of 1D+4DVAR data assimilation of radar reflectivity in JNoVA. *CAS/JSC WGNE Res. Activ. Atmos. Oceanic Modell.,* **41**, in press.

Ishida, J., 2007: Development of a hybrid terrain-following vertical coordinate for JMA Non-hydrostatic Model. *CAS/JSC WGNE Res. Activ. Atmos. Oceanic Modell.*, **37**, 0309 – 0310.

Ishikawa, Y., 2010: Data Assimilation of GPS Precipitable Water Vapor into the JMA Mesoscale Numerical Weather Prediction Model. *CAS/JSC WGNE Res. Activ. Atmos. Oceanic Modell.*, **40**, 0113-0114.

Ishimizu, T. and M., Ujiie, 2010: Experimental operation of a high-resolution local forecast model at JMA (3). *CAS/JSC WGNE Res. Activ. Atmos. Oceanic Modell.*, **40**, 0513 – 0514.

Saito, K., T. Fujita, Y. Yamada, J. Ishida, Y. Kumagai, K. Aranami, S. Ohmori, R. Nagasawa, S. Kumagai, C. Muroi, T. Kato, H. Eito and Y. Yamazaki, 2006: The operational JMA Nonhydrostatic Mesoscale Model. *Mon. Wea. Rev.*, **134**, 1266 – 1298.

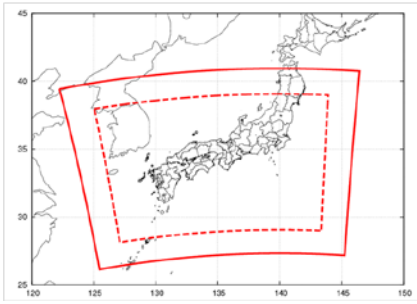

Fig. 1 LFM domain (dashed line) and LA domain (solid line)

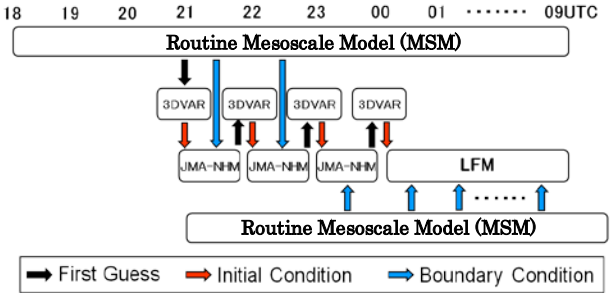

Fig. 2: Design of the LA rapid update cycle

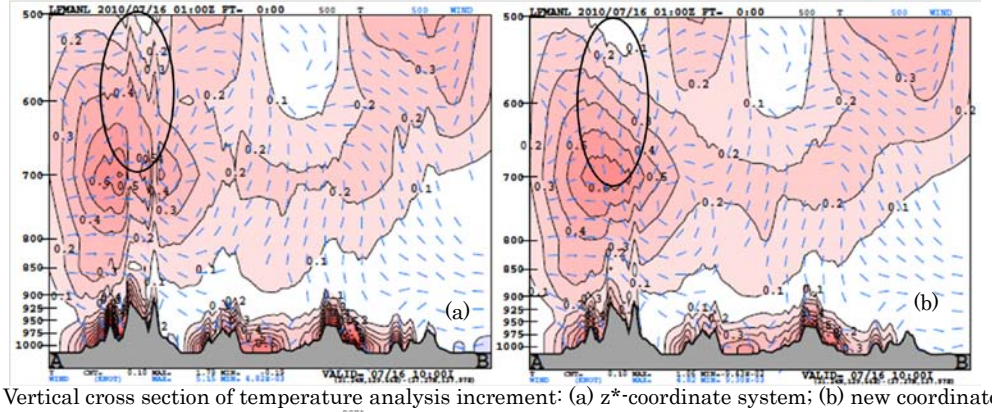

Fig. 3: Vertical cross section of temperature analysis increment: (a) z*-coordinate system; (b) new coordinate system

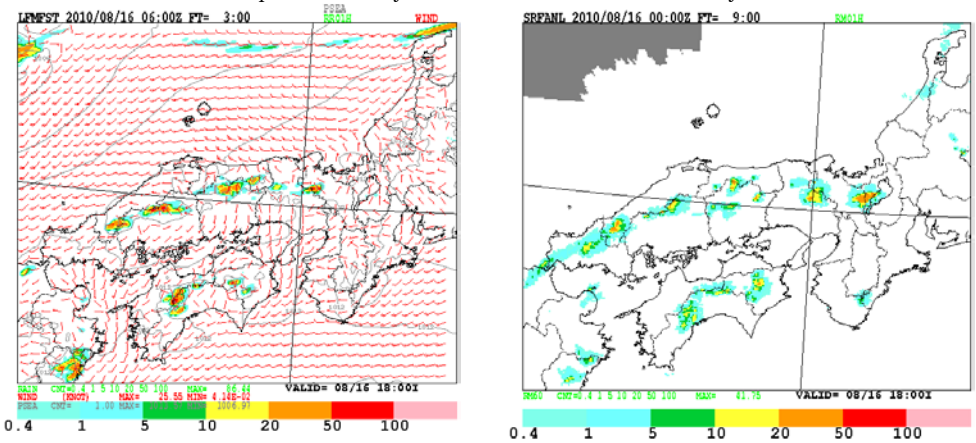

Fig. 4 1-h accumulated precipitation: (a) 3-h forecast from LFM; (b) observation

Development of 1D+4DVAR data assimilation of radar reflectivity in JNoVA

Yasutaka Ikuta[1] and Yuki Honda

Numerical Prediction Division, Japan Meteorological Agency

Japan Meteorological Agency (JMA) has been operating meso-scale model (MSM), and a four-dimensional variational (4DVAR) data assimilation system based on JMA non-hydrostatic model (JNoVA; Honda et al. 2005) to provide the initial condition of MSM. We have been developing a new approach of '1D+4DVAR' technique of data assimilation system using a radar reflectivity to improve analysis of water vapor and precipitation forecast. In the new approach, a one-dimensional (1D) pseudo observation data of relative humidity (RH) are retrieved by radar reflectivity, and retrieved RH data are assimilated as conventional data in JNoVA. Caumont et al. (2010) reported that the precipitation forecast is improved by using the combination of such 1D retrieval and a three-dimensional variational (3DVAR) data assimilation method (1D+3DVAR) in AROME.

The 1D retrieval method of the pseudo observation of RH employs a best estimate based on Bayes' theorem (Caumont et al. 2010). In the best estimate, the radar simulator (Ikuta and Honda 2010) plays an important role as an observation operator. The conditional expectation of RH is defined by:

$$E(x) = \int x \cdot p(y = y_o \mid x = x_{true})\, p(x = x_{true})\, dx = \sum_i x_i W_i(y_o) \Big/ \sum_j W_j(y_o) \qquad \text{with} \quad W_i \equiv \exp\left\{ -\frac{1}{2}(y_o - y_{s,i})^T R_{Z,ii}^{-1}(y_o - y_{s,i}) - J_p \right\},$$

where x_i is model state of RH, y_o is reflectivity observation, y_s is simulated reflectivity and W_i is weight. In particular, we have added penalty term J_p which is function of height innovation to the weight in this study. The x_i and W_i are given by supported database which is made from the radar simulator outputs (Fig. 1). The 1D+4DVAR data assimilation has an advantage of avoiding the difficulties such as estimating individual type of the hydrometeors from the radar reflectivity because of strongly nonlinear relation between reflectivity and these hydrometeors.

The analysis-forecast cycle experiment demonstrated an improvement of hydrometeors representation as an initial condition. Figure 2 shows that the representation of the simulated and observed reflectivity of Fukuoka radar site. The distribution of radar reflectivity simulated by the first guess is different from that of observed reflectivity, indicating that the first guess has displacement error of simulated hydrometeors distribution. This displacement error is successfully corrected after 1D+4DVAR data assimilation. A forecast experiment is conducted to compare the 33 hours MSM forecast with different analysis methods for the period from 20 July to 26 July 2009. As a result, the equitable threat score (Fig. 3a) and bias score (Fig. 3b) of 1D+4DVAR experiment (referred to as "Test") show an improvement of precipitation forecast than 4DVAR experiment without radar reflectivity assimilation (referred to as "Control") in the early hours of the forecast. Especially, the sudden drop of bias score around FT=3 in the Control experiment is improved in the Test experiment, suggesting that the 1D+4DVAR data assimilation improves analysis of water vapor field (Fig. 4).

References

Honda, Y., M. Nishijima, K. Koizumi, Y. Ohta, K. Tamiya, T. Kawabata and T. Tsuyuki, 2005: A pre-operational variational data assimilation system for a non-hydrostatic model at the Japan Meteorological Agency: Formulation and preliminary results. *Quart. J. Roy. Meteor. Soc.*, **131**, 3465-3475.

Caumont, O., V. Ducrocq, É. Wattrelot, G. Jaubert, S. Pradier-vabre, 2010: 1D+3DVar assimilation of radar reflectivity data: a proof of concept. *Tellus A, Volume* **62**, 173–187.

Ikuta, Y. and Y. Honda, 2010: Fuzzy Verification of Hydrometeors in a High-resolution Model Using a Radar Simulator. *CAS/JSC WGNE Res. Activ. Atmos. Oceanic Modell.*, **40**, 05.09 – 05.10

Yuter, S. E., and R. A. Houze Jr., 1995: Three-dimensional ki-nematic and microphysical evolution of Florida cumulo-nimbus. Part II: Frequency distributions of vertical velocity, reflectivity, and differential reflectivity. *Mon. Wea. Rev.*, **123**, 1941–1963.

[1] ikuta@met.kishou.go.jp

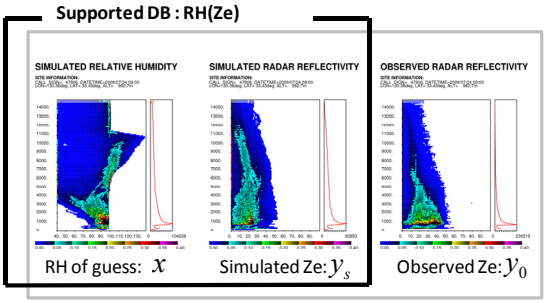

Fig. 1 CFADs (contour frequency by altitude diagram, Yuter and Houze 1995) of simulated RH, reflectivity and observed reflectivity. Supported database is composed by simulated RH and reflectivity.

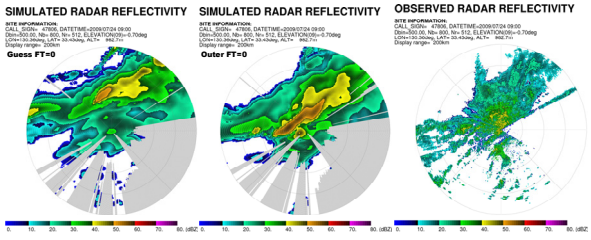

Fig. 2 PPI (plan position indicator) of elevation 0.7°. Simulated reflectivity by guess (left), simulated reflectivity by initial condition of MSM (middle), and observed reflectivity (right). The gray color region represent beam blockage by topography.

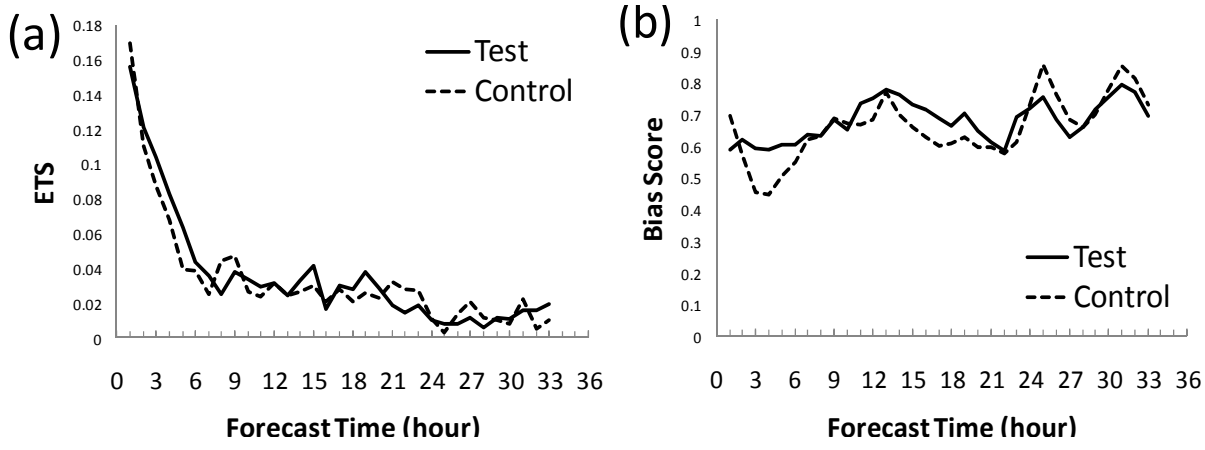

Fig. 3 Comparison of Test experiment and Control experiment of precipitation verification against RA. Time series of (a) equitable threat score (ETS) and (b) Bias Score. Solid line is the scores of Test, and dashed line is that of Control. Moreover, verification region is Japan, verification grid size is 20km and threshold is 10mmh^{-1}.

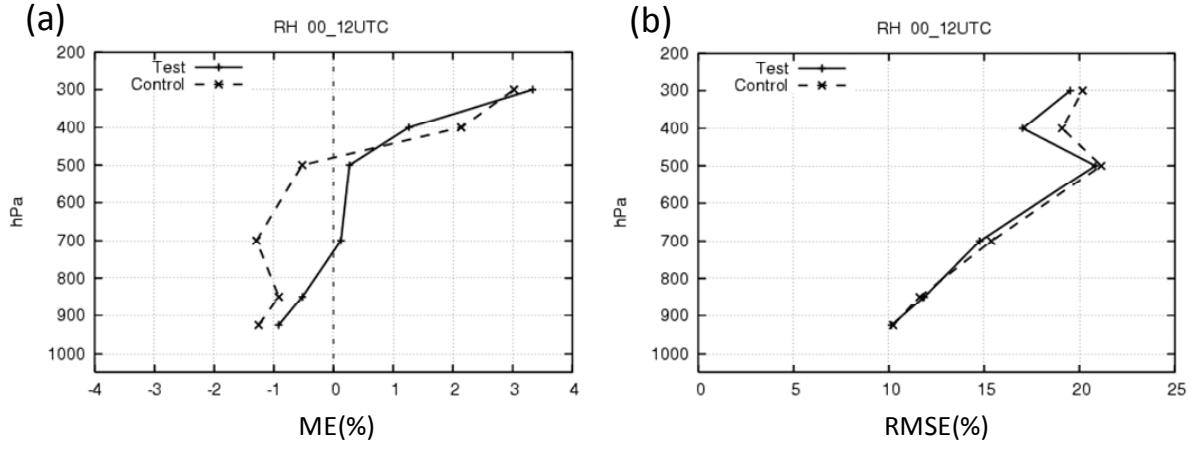

Fig. 4 Comparison of Test experiment and Control experiment of RH profile verification against sonde observation. (a) Mean error (ME) and (b) Root mean square error (RMSE). Solid line is the scores of Test, and dashed line is that of Control. Moreover, verification region is Japan and forecast time is 3 hours.

Cloudy radiance assimilation

with extension of control variables in 4D-Var

Toshiyuki Ishibashi
Meteorological Research Institute, Japan Meteorological Agency
E-mail: ishibasi@mri-jma.go.jp

1. Introduction

Direct assimilation of clear sky radiance data from satellites with four-dimensional variational (4D-Var) data assimilation systems (DASs) is one of the main factors in improvements of analysis and forecast accuracy. While, we know atmospheric disturbances often accompany clouds. Therefore, we can guess the radiance data in cloudy regions have ability to detect fast growing components of background errors, and reduce forecast errors significantly. However, the direct assimilation of radiances in cloudy regions (cloudy radiances) is difficult because, in the cloudy regions, the accuracy of first guesses is worse than that of clear sky radiances, and strong nonlinearity of the physical process concerned with water substances is exist.

In this letter, we describe the development of the direct assimilation of the cloudy radiances with extension of control variables in 4D-Var.

2. Extension of control variables in 4D-Var

We extend control variables of 4D-Var to include total cloud water content (TCW, the sum of cloud water content and cloud ice content) for the direct assimilation of cloudy radiances. Here, we use the Japan Meteorological Agency (JMA) global 4D-Var DAS.

First, we briefly describe the cloud processes of the global numerical weather prediction (NWP) model of JMA (JMA, 2007). The forecast variables of the model include TCW. The cloud scheme of the model is constructed from the probabilistic cloud scheme (Smith, 1990) and the Arakawa-Shubert scheme, and the scheme determines TCW and cloud cover simultaneously. TCW is divided into cloud ice and cloud water by the linear diagnostic function of temperature. The inner models of 4D-Var, the tangent linear model and the adjoint model, also include corresponding cloud schemes, however, in the routine system, initial values of perturbations and forcing of TCW are set to zero. Therefore, if we give the initial values and the forcing, these inner models can construct the time evolution part of the observation operators for cloudy radiances, and there is no need to construct new diagnostic operators which calculate cloud quantities from ordinary control variables.

Figure 1 shows scatter plots of linear and nonlinear time evolution of perturbations of TCW, cloud cover, and specific humidity. We can find explicit linearity

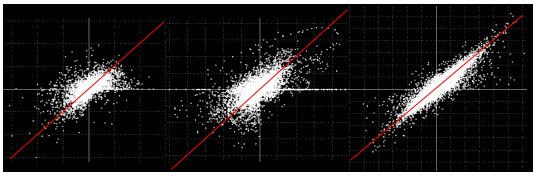

Figure 1. The tangent linearity of NWP model for TCW (left), cloud cover (center), and specific humidity (right). The red lines denotes the perfect tangent linearity.

for specific humidity and weaker but still explicit linearity for TCW and cloud cover.

To give adequate error covariance matrix for TCW is not an easy problem. Here, we take simple way as a first step. The background error covariance matrix of TCW is given as the same space correlation structure as that of specific humidity and variance is rescaled by one scalar coefficient. In following sections, this scalar coefficient is given as 10^{-3}.

3. Experimental Design

Here, we describe the experimental design to evaluate the extended 4D-Var for cloudy radiance assimilation, which is described previous section. We assimilate cloud affected AMSU-A radiances, channel 4 to 6, as cloudy radiance data. These data have information of clouds, however, not used in the JMA operational system. To see averaging property of these channels, Figure 2 shows Jacobian of averaged radiances in these channels. We find the main sensitivity altitudes for temperature, specific humidity, and cloud water are about 300hPa, 300hPa and 900hPa, and 900hPa, respectively. The sensitivity to cloud ice content for these channels can be ignored, since it is very small (figures not shown).

Analyses with three DASs (CNTL, CNTL-CLD, and TEST) are executed at 00UTC 20 Jul 2009. CNTL assimilates the original observation data with the original 4D-Var, CNTL-CLD assimilates the original data and cloudy radiances with the original 4D-Var, and TEST assimilates the original data and cloudy radiances with the extended 4D-Var. Three day forecasts from the three analysis fields are calculated and forecast accuracy are compared.

4. Experimental Results

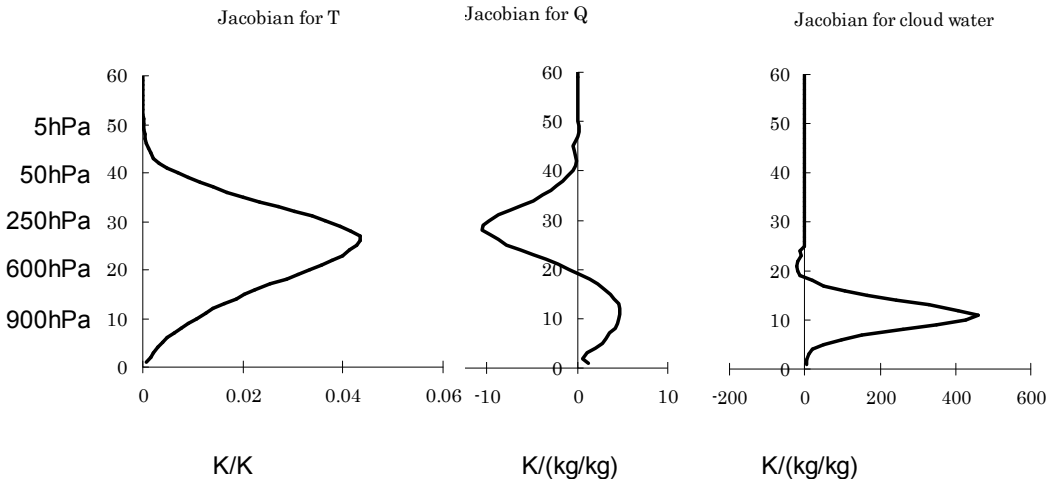

Figure 2. The averaged Jacobian of AMSU-A for channel 4, 5, 6. The left panel is Jacobian for temperature, the center is for specific humidity, and the right is for cloud water content.

Figure 3 shows the improvement rate of forecast RMSEs of CNTL-CLD and TEST from CNTL. Here, analyses generated by the original 4D-Var (CNTL) are used for truth. The figure shows TEST changes forecast accuracy from CNTL in mainly near 300hPa and 700hPa. These levels correspond to the sensitivity altitude of cloudy radiances (Figure 2). We find wide improvement area in the figure, although, error increases are found before 24 hours and after 60 hours at low levels. We can guess the error increases before 24 hours are not important because in this time analysis errors are not enough small compared with forecast errors differences. The figure also shows CNTL-CLD changes forecast accuracy from CNTL in near 300hPa and the low levels. We find wide improvement area above 700hPa in the figure, although, error increases are found after 24 hours at the low levels (mainly blow 900hPa).

The main difference of the forecast accuracy changes are the error increases in CNTL-CLD and the error decreases in TEST at the low levels. These altitudes correspond to the sensitivity levels of cloud water content, and we can guess the improvement of TEST is due to the adequate treatment of cloud water content sensitivity.

5. Future plans

In this letter, we have described the extension of 4D-Var for cloudy radiance assimilation. Future plans are as follows; First, one month long OSEs for statistically significant evaluation are needed. Secondly, the processes of the forecast accuracy changes caused by the cloudy radiance assimilation should be understood. Thirdly, the error covariance matrix of TCW should be set more adequately. Finally, more strong cloud affected or rain affected radiances (microwave imagers and infrared sensors) will be tested.

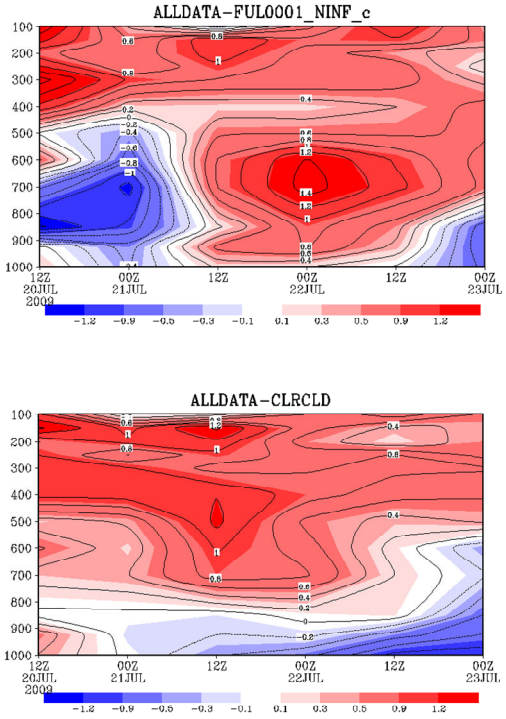

Figure 3. The improvement rate of the forecast RMSEs for temperature. The upper panel is the improvement rate of TEST, defined as (CNTL–TEST)/CNTL. The bottom panel is the improvement rate of CNTL-CLD, (CNTL–CNTL-CLD)/CNTL. The vertical axis is the pressure altitudes, and the horizontal axis is the forecast days (three days).

Effects of basic state update in the JMA global 4D-Var

Toshiyuki Ishibashi
Meteorological Research Institute, Japan Meteorological Agency
E-mail: ishibasi@mri-jma.go.jp

1. Introduction

Analyses of the atmosphere based on variational schemes (4D-Var, 3D-Var) are executed with optimization algorithms (the quasi Newton method, the conjugate gradient method) using gradient of the cost function. If the tangent linear approximation of the observation operator is valid around a basic state, the cost function becomes quadratic form. The quadratic form of the cost function is desirable for the optimization problem, and for operational data analysis systems (DASs) to be stable and keep high accuracy. Further more, in this case, since the DAS becomes a linear system, we can derive the analytical solution easily, and linear analyses of analysis and forecast results are possible. While, the DAS have to treat nonlinearity of the observation operator because observations based on remote sensing (satellite radiances, RADAR, GPS) have contributed to analysis and forecast accuracy largely, and nonlinearity of observation operators of these data is stronger than that of conventional direct observations. Furthermore, cloud and rain affected observations may bring significant improvement of analysis and forecast accuracy.

Therefore, both linearity and nonlinearity of observation operators are requested in DASs. The basic state update in incremental 4D-Var (Courtier et al. 1994) is an answer of these contradistinctive requests. The basic state update has been used in several numerical weather prediction centers, and analyses by the adjoint-based observation impact estimation method also shows effectiveness of the method (Trémolet 2008). We describe the first test of the basic state update in the Japan Meteorological Agency (JMA) global 4D-Var DAS.

2. Formulation of basic state update

The incremental 4D-Var with the basic state update is formulated as follows;

$$J^m \cong \frac{1}{2}\left(\delta\mathbf{x}^m + \mathbf{b}^m\right)^T \mathbf{B}^{-1}\left(\delta\mathbf{x}^m + \mathbf{b}^m\right) + \frac{1}{2}\left(\mathbf{d}^m - \mathbf{H}^m\delta\mathbf{x}^m\right)^T \mathbf{R}^{-1}\left(\mathbf{d}^m - \mathbf{H}^m\delta\mathbf{x}^m\right),$$

$$\delta\mathbf{x}^m = \left(\mathbf{B}^{-1} + \mathbf{H}^{mT}\mathbf{R}^{-1}\mathbf{H}^m\right)^{-1}\mathbf{H}^{mT}\mathbf{R}^{-1}\mathbf{d}^m - \left(\mathbf{B}^{-1} + \mathbf{H}^{mT}\mathbf{R}^{-1}\mathbf{H}^m\right)^{-1}\mathbf{B}^{-1}\mathbf{b}^m,$$

where, J is the cost function, $\delta\mathbf{x}$ is the analysis increment vector, $\mathbf{y}$ is the observations, $\mathbf{d}$ is the departure vector (differences between observations and guesses), $\mathbf{B}$ is the back ground error covariance matrix, $\mathbf{R}$ is the observation error covariance matrix, $\mathbf{H}$ is the tangent linear observation operator. The superscript m denotes m-th basic state update concerned quantity, and $\mathbf{b}$ is the differences between the basic field and the background field.

To recalculate departure values using a high-resolution outer model for the basic state update is computationally expensive. Here, we take more simple way using an assumption about representation errors, which is usually used in departure value calculations. First, the resolution that we can analyze is that of an inner model space. Therefore, the departure values must be differences between observations and guesses in inner model resolution. However, such observations with inner model resolution are not exist, so differences between guesses in outer model space and original observation values are used usually. This is the same as the assumption that high wave number components of guesses and observations are canceled out by the subtraction. If we separate observations into the low and the high resolution parts formally. This assumption is written, as follows;

$$\mathbf{y} = \mathbf{y}^L + \delta_y; \quad H^h\left(\mathbf{x}_b^h\right) = H^L\left(\mathbf{x}_b^L\right) + \delta_b$$
$$\mathbf{d}_b^h = \mathbf{y}^L - H^L\left(\mathbf{x}_b^L\right) + \left(\delta_y - \delta_b\right) \cong \mathbf{y}^L - H^L\left(\mathbf{x}_b^L\right) = \mathbf{d}_b^L,$$

where, the superscripts L, h, and the subscript b denote low resolution, height resolution, and background field concerned quantity, respectively. H(x) is observation operator. The last approximate equivalence means we ignore the differences between the deltas, and this corresponds to the assumption. Therefore, hypothetical low-resolution observation can be calculated as the sum of high resolution departures and low-resolution first guesses. This form is the same as the equations found in Courtier et al. (1994) and Ishikawa and Koizumi (2002, in Japanese). Using this expression, basic state updated departure values for inner resolution are given as follows;

$$\mathbf{d}_g^L = \mathbf{y}^L - H^L\left(\mathbf{x}_g^L\right) \cong \left(\mathbf{d}_b^h + H^L\left(\mathbf{x}_b^L\right)\right) - H^L\left(\mathbf{x}_g^L\right),$$

where, subscript g denotes updated basic state concerned quantity.

3. Experiment

We have implemented the basic state update scheme to the low-resolution version of the JMA global 4D-Var. An analysis and succeeding three day forecast are performed with the scheme at 00UTC 20 Jul 2009 to evaluate the effectiveness of the scheme.

The experimental results are as follows. Figure 1 shows the decreases of observation terms of the cost function for each observation dataset after the basic state update. The most large reduction rate is found in radiance data, about 12% reduction, and the next is GPS radio occultation data and relative humidity direct observations. These observations correspond to complex observation operators or water vapor concerned observations. We can also find the decreases of cost function in temperature and winds concerned direct observations. This is because these observation operators also include the NWP model as the time evolution operator. Figure 2 shows changes in forecast accuracy due to the basic state update. The figure shows forecast errors for temperature are reduced almost all area. Forecast error reduction in winds and geo-potential height is also found (Figures not shown). However, the forecast errors of humidity in the mid troposphere has the trend to increase.

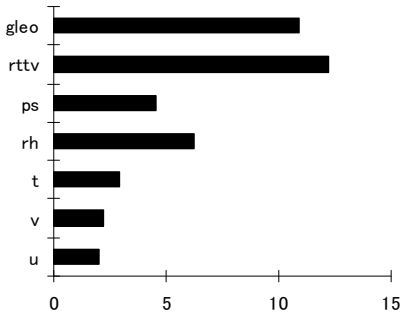

Figure 1. The decreases of observation terms of the cost function for each observation dataset due to the basic state update. The horizontal axis is the decrease rate (%), the vertical axis is observation dataset name. gleo is the GPS radio occultation data, rttv is radiances, ps is surface pressure, rh is relative humidity, u is the zonal wind, and v is the meridional wind.

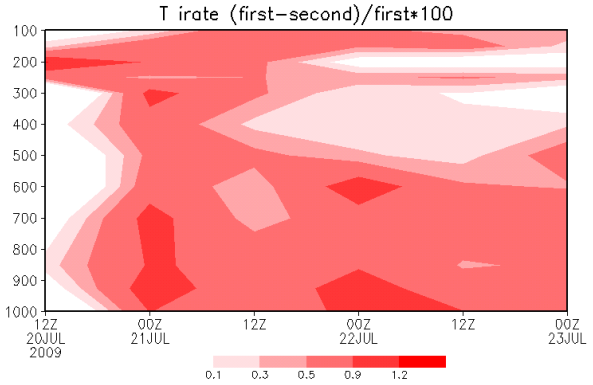

Figure 2. The improvement rate of forecast RMSE for temperature. The improvement rate is defined as (CNTL–TEST)/CNTL, where, TEST is with the basic state up date, and CNTL is without it. The horizontal axis is the forecast days (three days), the vertical axis is the pressure altitudes (hPa). The red shade denotes more than 0.1% improvement areas due to the basic state update.

An assimilation experiment of GPS-derived water vapor observations on a local heavy rainfall event

Takuya KAWABATA, Yoshinori SHOJI, Hiromu SEKO, Kazuo SAITO
(Meteorological Research Institute / Japan Meteorological Agency)

1. Introduction

The Meteorological Research Institute of the Japan Meteorological Agency (JMA) has been developing a nonhydrostatic cloud-resolving 4DVAR assimilation system (NHM-4DVAR; Kawabata et al. 2011) based on the JMA operational mesoscale model (NHM). The aim of this development is to investigate mechanisms of strong convection. A forward model of NHM-4DVAR is a full nonlinear JMA-NHM (Saito et al. 2007), while the tangent linear and the adjoint models consider perturbations to the dynamics and the warn rain cloud microphysics process. Horizontal resolution is 2 km.

In this paper, an assimilation experiment on a local heavy rainfall event occurred on 19 August 2009 in Okinawa Island, Japan is presented, and comparisons of assimilation methods of GPS data (precipitable water vapor (PWV), GPS zenith total delay (ZTD), and GPS slant total delay (STD)) data are discussed.

2. GPS-derived water vapor observations

First, slant total delay amounts of radio waves from GPS satellites to receivers are observed at each GPS observation site (STD). It is possible to observe several STDs at one GPS observation site at the same time. These data are mapped to the zenith direction and averaged (ZTD). Since radio-wave delay is affected by dry atmosphere and water vapor (Eq. 1) and these delays are separated, we can obtain information on accumulated wet atmosphere (PWV). Figure 1 illustrates above methods. PWV and ZTD have information on water vapor in the zenith direction only above the observation site, while are affected by several factors of atmospheric conditions (pressure, temperature, and water vapor). On the other hand, STD has vertical and horizontal information of several factors of the atmosphere. This characteristic of STD is advantageous to reproduce small scale phenomena (e.g., cumulonimbus), especially, for a high resolution assimilation system.

We have developed the assimilation method of STD; Delay amount is calculated with Eq. (1) at each model grid box and integrated along a radio wave path. Since the model top height of NHM-4DVAR is about 20,000 m, we assume that delay amount above the model top level

$$(n-1)\times 10^6 = K_1\left(\frac{P_d}{T}\right) + K_2\left(\frac{P_v}{T}\right) + K_3\left(\frac{P_v}{T^2}\right) \quad \text{..... (1)}$$

n: refractivity, Pd: partial pressure of dry atmosphere, Pv: partial pressure of water vapor, T: temperature, K1, K2, K3: constants.

decreases exponentially and becomes zero at 200 km height Moreover, we introduced the observational error of STD depending on elevation angle of slant path.

Figure 2 show an example of delay amount at each model grid calculated with Eq. (1). These are distributed along radio slant path. Here, cold colored points show small amount of delay and locate in high levels, while

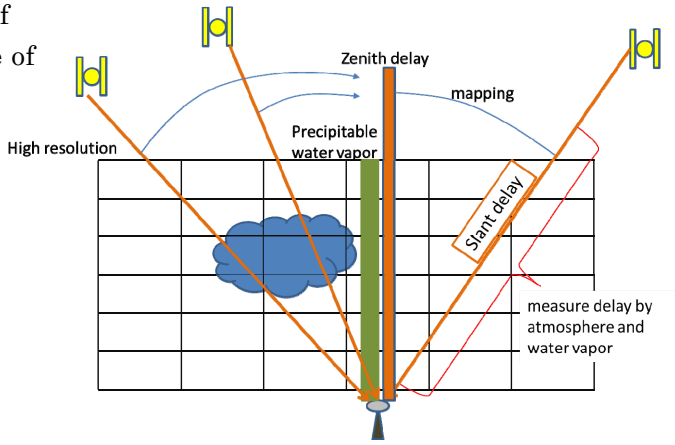

Figure 1. schematic of GPS-derived water vapor observations.

warm colored points show large amount of delay and locate in low levels. In addition, they distribute horizontally wide, thereby, STD provides horizontal and vertical atmospheric information.

3. Assimilation experiment

Impact test of GPS observation assimilation was conducted for a local heavy rainfall event on 19 August 2009 in Okinawa Island, Japan. A 1-h assimilation window was set from 11 to 12 JST (Japan Standard Time). After the assimilation, we conducted a 3-h forecast from 11 to 14 JST. GPS observations were processed according to Shoji (2009). Hereafter, the case in which first-guess field was used is called as 'BCK', the case in which GPS precipitable water vapor was assimilated is called as 'PWV', the case in which GPS zenith total delay was assimilated is called as 'ZTD', and the case in which GPS slant total delay was assimilated is called as 'STD'.

Figure 3 shows 1-h accumulated rainfall amount at 14 JST. In observation (Fig. 3a), intense rainfalls over 20 mm h^{-1} is seen in the southwest of Okinawa Island, corresponding rainfall areas are forecasted in STD (Fig. 3b). Only weak rainfalls are seen in PWV (Fig. 3c), though rainfall distribution of PWV and ZTD are slightly improved compared with BCK (Fig. 3d). Namely, two intense rainfall cells southwest of Okinawa Island are seen in the observation and PWV, but only one cell is seen in BCK. Result of ZTD was similar to that of PWV (not shown). From these results, we can say that assimilation of GPS observation improves the heavy rainfall forecast. Especially, STD data have a positive impact on intensity on the heavy rainfall forecast in a high resolution assimilation system.

Reference

Kawabata, T., T. Kuroda, H. Seko and K. Saito, 2011: A cloud-resolving 4D-Var assimilation experiment for a local heavy rainfall event in the Tokyo metropolitan area. *Mon. Wea. Rev.* 139. (in press).

Saito, K., J. Ishida, K. Aranami, T. Hara, T. Segawa, M. Narita, and Y. Honda, 2007: Nonhydrostatic atmospheric models and operational development at JMA. *J. Met.Soc. Japan*, 85B, 271–304.

Shoji, Y. 2009: A Study of Near Real-time Water Vapor Analysis Using a Nationwide Dense GPS Network of Japan, *J. Met. Soc. Japan*, 87, 1, 1-18.

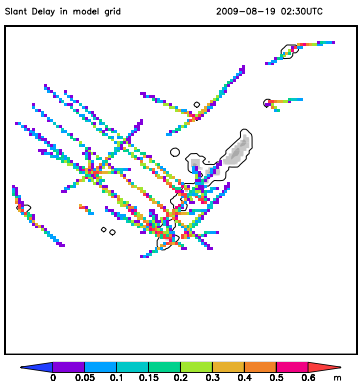

Figure 2. Horizontal distribution of delay amount on model grids. Delay amount on each model grid calculated with Eq. (1). Cold colored points show small amount. Warm colored points show large amount.

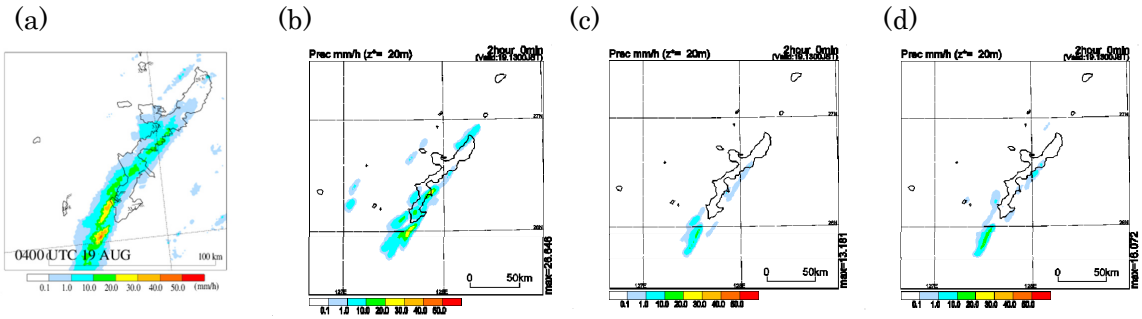

Figure 3. 1-h accumulated rainfall amount of (a) Observation, (b) STD, (c) PWV, (d) BCK.

Operational Use of Satellite Radiance in JMA Mesoscale Analysis

Masahiro Kazumori
Numerical Prediction Division, Japan Meteorological Agency
E-mail: kazumori@met.kishou.go.jp

In order to assimilate observed satellite radiance in JMA's operational Numerical Weather Prediction (NWP), a fast radiative transfer model, RTTOV [1], was integrated into the JMA operational mesoscale 4D-Var system [2] as a satellite radiance observation operator. Clear sky radiance data are assimilated in the initial implementation. The radiance assimilation scheme was tested with operationally available satellite radiance observations such as AMSR-E, TMI, SSMIS, AMSU-A/B, MHS and MTSAT data. In this test, temperature retrievals from ATOVS and Total Column Water Vapor (TCWV) retrievals from microwave imagers were removed. Similar quality control of radiance data in JMA's global analysis [3] was applied for this system. In radiative transfer calculation, atmospheric profiles were extrapolated using the lapse rate of the U.S. standard atmosphere from the mesoscale model's top height (22km). The horizontal data thinning distance was also set as 45km to fit the high-resolution mesoscale model (the model's horizontal resolution is 5km for the outer model and 15km for the inner model). Bias correction coefficients determined in the variational bias correction scheme of JMA's global analysis are used in this system.

The radiance assimilation brought considerable improvements, especially in tropospheric analysis of temperature/humidity and short-range forecasts. These improvements were confirmed through verification using radiosonde and surface observation in Japan [4]. Assimilations of radiance from various microwave imagers and humidity sounders produced TCWV analysis increments similar to those of the retrieved TCWV assimilation. As radiance assimilation enables the use of satellite data without the need for a retrieval process, DMSP F-16 and F-17 SSMIS radiances were newly incorporated into the system. These data brought a significant moisture analysis improvement and strengthened the TCWV contrast between moist and dry areas in typhoon events (Figure 1).

In addition to improvements in the analysis field, enhancements in track forecasting for low-pressure systems and intensity forecasting were also confirmed. Simulated MTSAT infrared images from analysis and forecasting in radiance assimilation showed features similar to those of real MTSAT infrared images. Forecasting for typhoon intensity and maximum wind speeds was also improved (not shown). Enhanced forecasting of heavy rainfall was confirmed in verification with rainfall analysis from ground-based radar and rain gauges in Japan (Figure 2).

Based on these findings, the radiance assimilation scheme was implemented in JMA's operational mesoscale NWP system on December 13, 2010.

References

[1] Saunders, R. W., 2008: RTTOV-9 Science and Validation Report. EUMETSAT, pp. 74.
[2] Honda, Y. and K. Sawada, 2009: "Upgrade of the Operational Mesoscale 4D-Var System at the Japan Meteorological Agency," *CAS/JSC WGNE Res. Activ. Atmos. Oceanic Modell.,* **39**, 1.11 – 1.12.
[3] Kazumori, M., 2009: "The Impacts of an Improved Quality Control and Ocean Emissivity Model for Microwave Radiance Assimilation in the JMA Global 4D-Var Data Assimilation System," *CAS/JSC WGNE Res. Activ. Atmos. Oceanic Modell.,* **39**, 1.19 – 1.20.
[4] Kazumori, M., 2010: "Initial Results of a Direct Radiance Assimilation Experiment in the JMA Mesoscale 4D-Var Data Assimilation System," *CAS/JSC WGNE Res. Activ. Atmos. Oceanic Modell.,* **40**, 1.19 – 1.20.

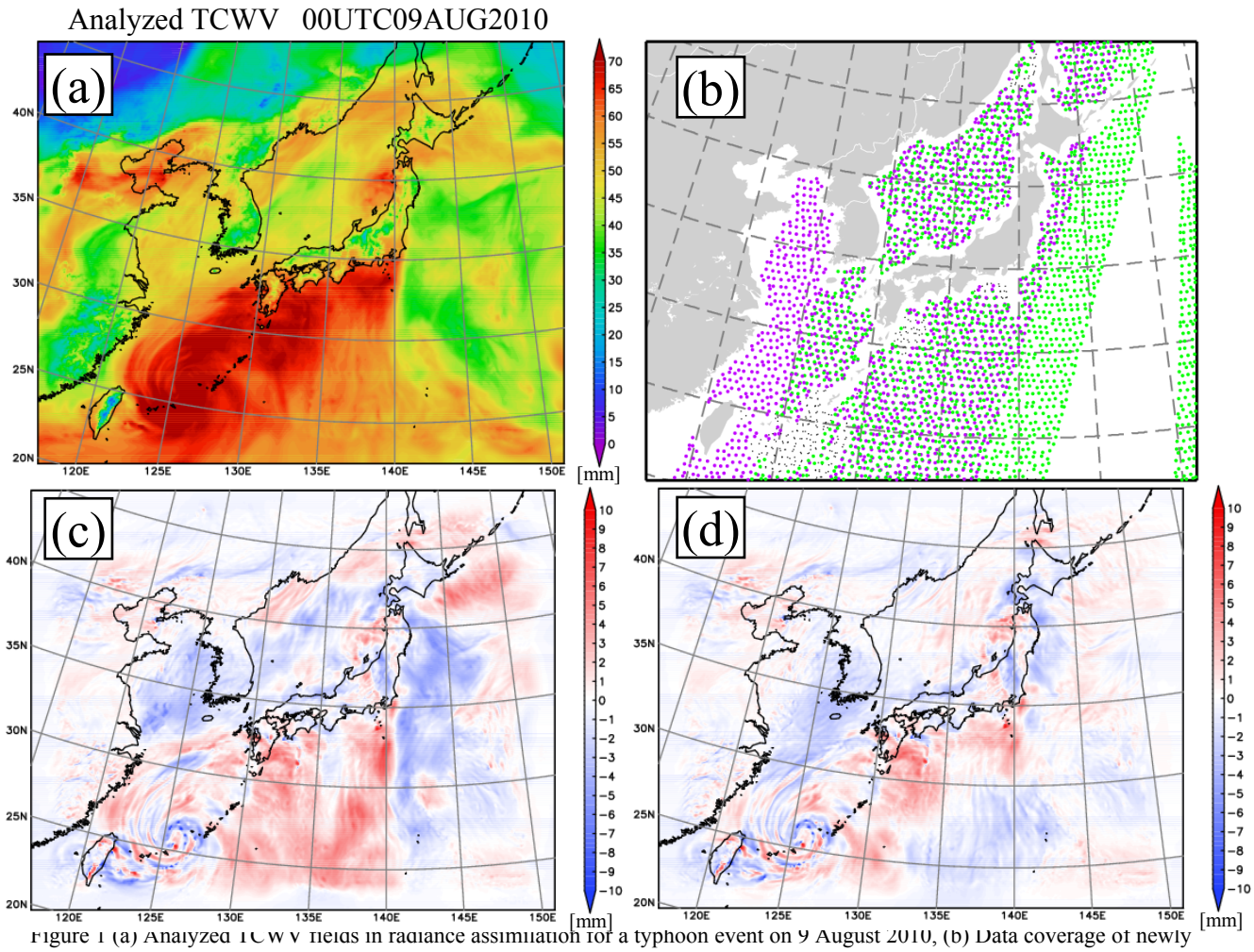

Figure 1 (a) Analyzed TCWV fields in radiance assimilation for a typhoon event on 9 August 2010, (b) Data coverage of newly added SSMIS radiance data – F-16 (green), F-17 (purple); (c) analysis increment for TCWV in radiance assimilation; (d) analysis increment for TCWV in retrieval assimilation

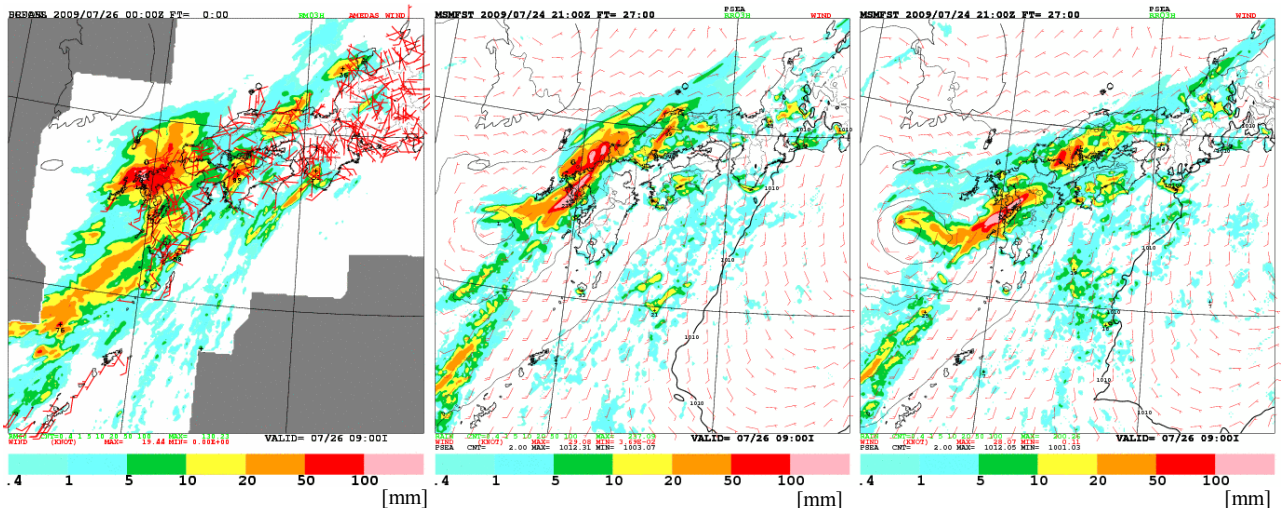

Figure 2 Three-hourly accumulated precipitation of 27-hour forecasts from 24 July 2009 with an initial time of 21 UTC. From the left, analyzed precipitation, forecasting of radiance assimilation and that of retrieval assimilation are shown.

Recent Modifications of Tropical Cyclone Bogus Data in the JMA Global and Meso-scale Data Assimilation Systems

Akira Okagaki[1], Hiroshi Sako[2]
Numerical Prediction Division, Japan Meteorological Agency

In JMA's global and meso-scale NWP systems, a typhoon-bogus scheme is applied to initialization for tropical cyclones (TCs) over the western North Pacific. In this scheme, a typical TC structure is generated based on real-time TC analysis at RSMC Tokyo, and pseudo-observation data (i.e., bogus data) extracted from this structure are deployed around the TC. The bogus data are assimilated in each NWP system.

Introduction of a bogus data adjustment function

In recent years, the accuracy of the first-guess fields in the operational analysis has been improved by the introduction of new satellite data and a sophisticated data assimilation system. This has reduced the relative accuracy of the bogus data to first-guess fields, and the assimilation of too many bogus data could impair the accuracy of analysis. To deal with this issue, a bogus data adjustment function has been introduced. With this function, the number of bogus data can be adjusted according to the distance from the TC's central position in the TC analysis to the one in the first guess. In many cases, the number of bogus data is greatly reduced compared with before, and these data are deployed only in the vicinity of the TC center.

Experiments and Results

For the global NWP system, data assimilation and forecast experiments were conducted prior to actual operation. The level of TC track prediction error was clearly reduced as a result of using the improved typhoon-bogus scheme (Figure 1). The new scheme was incorporated into the operational global NWP system in April 2010.

Introduction into the meso-scale NWP system

An almost-identical scheme was incorporated into the operational meso-scale NWP system in September 2010. One additional change for the meso-scale system is the timing of bogus data generation. Previously, these data were prepared for the start of the assimilation window (at a point three hours before the analysis time). In the new scheme, the data are prepared for the end of the assimilation window (at the analysis time). This allows the system to use the latest TC analysis data. However, since the meso-scale data assimilation process is started only 50 minutes after the analysis time, the real-time TC analysis data sometimes cannot be delivered in time. Any data delivered late will be used in the next data assimilation process at three hours later. TC track forecast error in experiments using this new scheme

[1] E-mail: a-okagaki@met.kishou.go.jp
[2] E-mail: h-sakou@met.kishou.go.jp

was reduced (Figure 2).

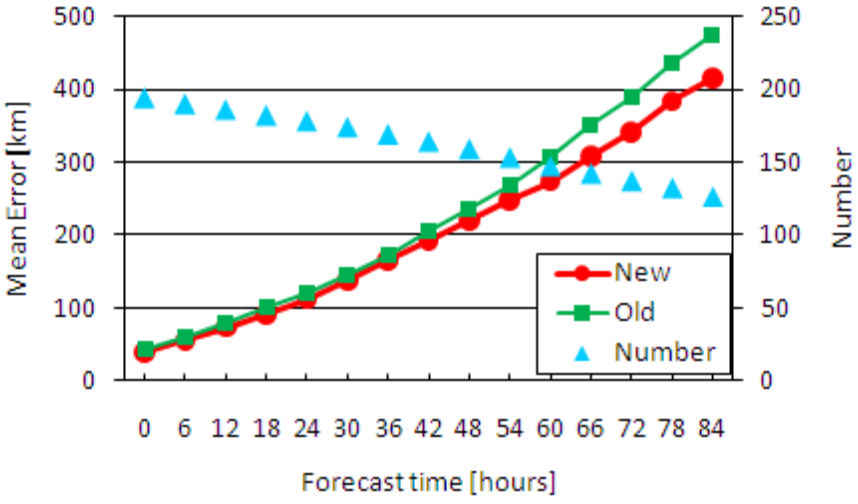

Figure 1. Mean track forecast errors (km) for TCs in RSMC Tokyo's area of responsibility from 25 September to 25 October, 2009, according to the global NWP system. The red line shows errors of TC track prediction with the improved typhoon-bogus scheme, and the green line shows those with the old one. The level of error is clearly lower with the improved scheme. The blue triangles denote the number of verification samples.

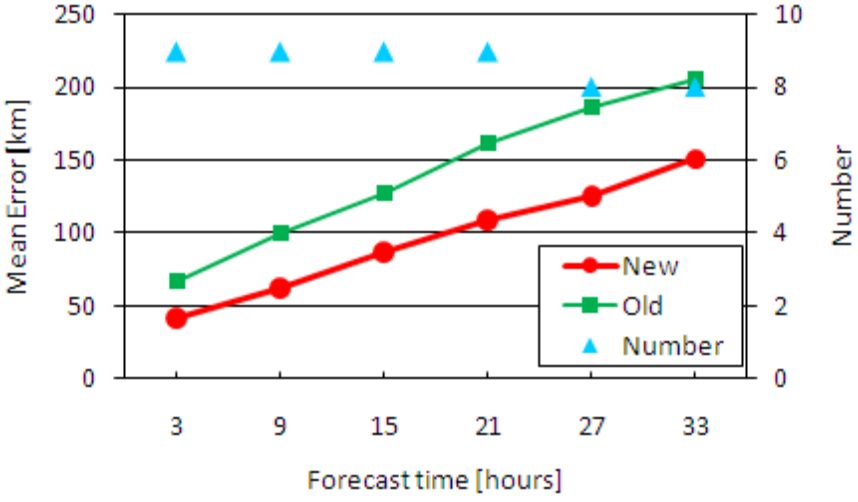

Figure 2. As Figure 1, but for meso-scale NWP system. The target typhoon is Typhoon KROVANH (T0911) and the study period is from 28–30 August, 2009.

Assimilation of COSMIC GPS-RO data for the JMA Global Spectral Model

Eiji OZAWA

Numerical Prediction Division, Japan Meteorological Agency

E-mail: ozawa@met.kishou.go.jp

1 Introduction

The Japan Meteorological Agency (JMA) started the assimilation of GPS radio occultation (GPS-RO) refractivity data from the COSMIC mission for the operational Global Spectral Model (GSM) on November 1, 2010. COSMIC data have been provided since February 8, 2010, via the Internet as it was possible to acquire them earlier than through GTS. This paper presents the assimilation configurations and pre-operational test results.

2 Bias correction for assimilation of GPS-RO data

GPS-RO refractivity data exhibit systematic biases in the troposphere against first-guess fields from GSM forecasts. Figure 1 shows the refractivity departures (O-B) between GPS-RO and the first guess with the same specifications as operation before bias correction. It was found that one of the reasons for such biases was that, rather than the virtual temperature, the temperature with piled-up height corresponding to GPS observations was used with reference to the refractivity of the first guess. Figure 2 shows the same situation as Fig. 1, but with virtual temperature for piled-up height. Figure 3 also shows the same situation as Fig. 1, but after bias correction, and Fig. 4 shows the same situation as Figure 2, but after bias correction.

Biases are corrected using linear regression equations. The regression coefficients are estimated with the Kalman filter for every analysis, and the predictors for bias correction are latitude, height and refractivity. The bias-corrected refractivity data are assimilated into the height range of 7 – 30 km. Observation errors and bias correction coefficients are defined independently in five latitudinal bands (90 – 60°S, 60 – 20°S, 20°S – 20°N, 20 – 60°N, 60 – 90°N), and observation errors are also defined as a function of height.

3 Assimilation experiments and results

Observation system experiments for COSMIC GPS-RO refractivity data were conducted in September 2009 and January 2009 as pre-operational tests. The control experiment (CNTL) had the same configuration as the operational GSM, and the COSMIC data were also assimilated in the test experiment (TEST). Figures 5 and 6 show differences in the zonal mean RMS errors between CNTL and TEST in 72-hour geo-potential height forecasts against their own initial fields for September 2009 and January 2009, respectively. The red areas are those where the root mean square (RMS) errors are smaller in TEST than in CNTL, which indicates forecast improvement from the assimilation of COSMIC GPS-RO data. Such improvement in the 72-hour forecast period is seen in most regions except around the Antarctic in the January experiment, although no such clear improvement is observed in the September experiment.

4. Acknowledgements

We would like to thank UCAR and NSPO for their provision of the COSMIC data used in this work.

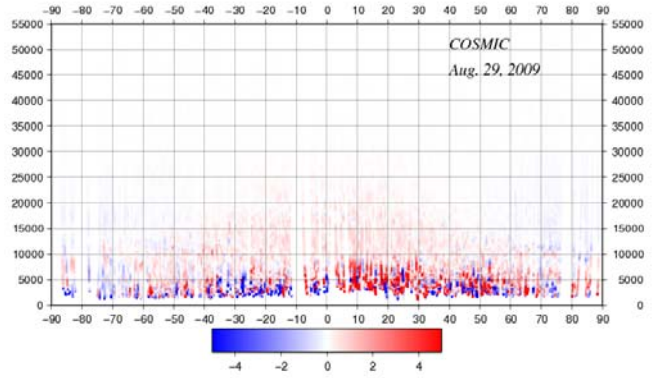

Fig. 1: COSMIC GPS-RO refractivity departures (O-B) between GPS-RO and the first guess. The vertical axis shows the height (m), and the horizontal axis shows the latitude (degrees). Red indicates positive departures, and blue indicates negative departures.

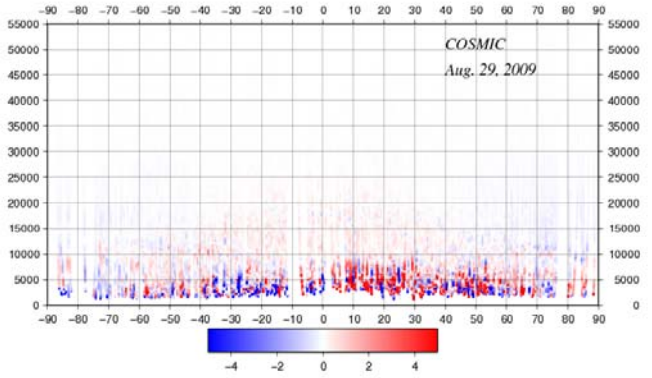

Fig. 2: As per Fig. 1, but with virtual temperature for piled-up height corresponding to GPS observation with reference to the refractivity of the first guess

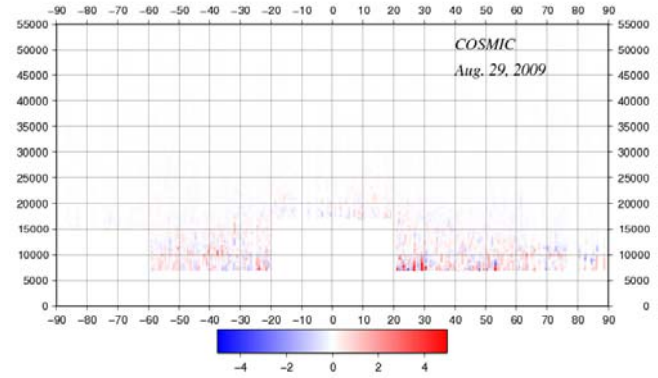

Fig. 3: As per Fig. 1, but after bias correction and quality control

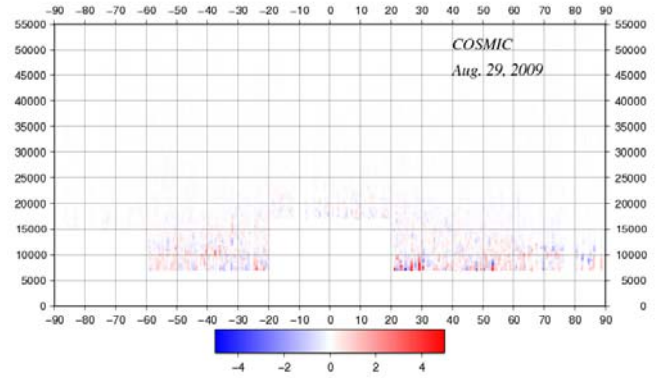

Fig. 4: As per Fig. 2, but after bias correction and quality control

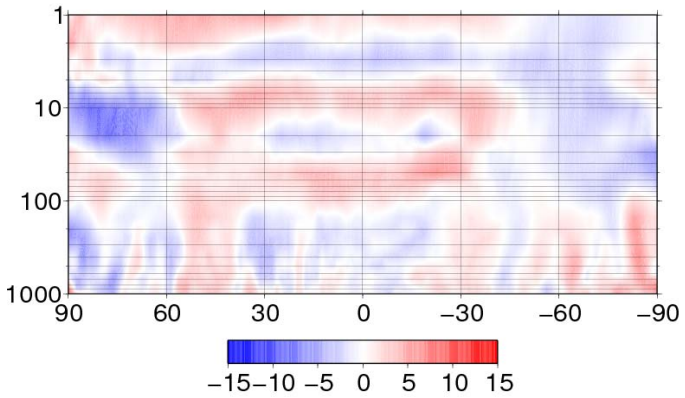

Fig. 5: Differences in zonal mean RMS errors between CNTL and TEST in 72-hour geo-potential height forecasts for September 2009. The vertical axis shows pressure (hPa), and the horizontal axis shows latitude (degrees). Red indicates improvement from the assimilation of COSMIC GPS-RO data, and blue shows deterioration.

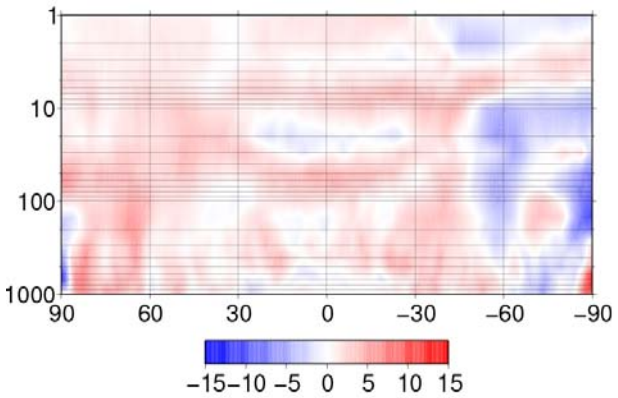

Fig. 6: As per Fig. 5, but for January 2009

The Concordiasi project over Antarctica

F. Rabier (1), A. Hertzog (2), Ph. Cocquerez (3), S. A. Cohn (4), L. Avalonne (5), T. Deshler (6), J. Haase (7),B. Brioit (2), F. Danis (2), F. Vial (2), A. Doerenbecher (1), V. Guidard (1), D. Puech (1),H. Cole (4), J. Fox(4), T. Hock (4), D. Parsons (4), J. VanAndel(4),L. Kalnajs (5), C. Genthon (8)

(1) Centre National de Recherches Météorologiques, CNRS and Météo-France, France ; (2) Laboratoire de météorologie dynamique, Ecole Polytechnique, CNRS, France ; (3) Centre National d'Etudes Spatiales, France ; (4) National Center for Atmospheric Research, USA ; (5) Laboratory for Atmospheric and Space Physics, University of Colorado, USA; (6) Department of Atmospheric Sciences, University of Wyoming, USA; (7) Department of Earth and Atmospheric Sciences, Purdue University, USA; (8) Laboratoire de Glaciologie et Géologie de l'Environnement, France

Corresponding email address : florence.rabier@meteo.fr

Concordiasi is an international effort organized around several observation campaigns in Antarctica, and its main scientific objectives are:to improve the assimilation in numerical weather prediction (NWP) models of infrared radiances provided by IASI-like hyperspectral spaceborne sounders over icy surfaces; to enhance the representation of polar processes in numerical models, and in particular to improve the simulation of precipitations, clouds, so as to better describe the mass budget of ice sheets; to advance our knowledge of microphysical and dynamical processes involved in stratospheric ozone loss, and to better understand the interactions between them.

To this end, a campaign of enhanced radiosoundings and surface measurements has taken place in 2008 and 2009 at Concordia, the French-Italian station on the Antarctic plateau. Radiosoundings were performed at Concordia, phased with the passage of the MetOp satellite (carrying IASI) over the station. It was found that the French NWP model was lacking in accuracy in its simulation of the surface temperature. Conversely, the combination of IASI and the model showed a positive impact, the combined values being much closer to those made in situ (figure 1).

The second part of the project is a long-duration balloon campaign which took place above Antarctica from September 2010 to early 2011. During this campaign, 19 12-m diameter superpressure balloons have been released in the stratospheric polar vortex from McMurdo station by the French space agency (CNES). The balloons flew around 17 km and carried up to 60 kg of instrumentation and flight devices. All balloons carried a small in-situ meteorological package. 13 balloons furthermore carried the driftsonde gondolas developed at NCAR. Each driftsonde gondola contained about 50 miniaturized dropsondes, which could be released individually on demand during the stratospheric balloon flight to provide high-resolution profiles of thermo-dynamic variables below the balloon. During the campaign, the dropsoundings were mainly phased with the MetOp passage above the balloons, in order to provide an in-situ truth that can be compared with the temperature profile retrieved from IASI observations. Some were also deployed in the so-called "sensitive regions" of numerical forecasts. The remaining 6 balloons carried scientific payloads devoted to tackle scientific issues linked to stratospheric dynamics and chemistry. This equipment included in-situ observation of ozone (with two instruments developed at LMD, France and at the University of Colorado), as well as particles with a particle counter developed by the University of Wyoming. These in-situ observations, performed on quasi-Lagrangian tracers of the flow, enabled us to follow the depletion of ozone during the spring season, and to assess the potential effect of mesoscale waves in triggering the formation of polar stratospheric clouds. In particular, the role of waves generated above the Antarctic Peninsula, which seems to be important for the formation of PSC leeward of the mountains, were monitored during the campaign. Furthermore, two of the balloons carried a GPS radio-occultation system developed by the University of Purdue to retrieve the temperature profile below the balloon several times per day. These observations, together with the in-situ meteorological measurements, will be used to diagnose the stratospheric wave activity globally over Antarctica.

References :

Rabier F., et al., The Concordiasi project in Antarctica, *Bull. Am. Meteorol. Soc.*, **91**, 69-86, doi: 10.1175/2009BAMS2764.1, 2010.

Acknowledgements: Concordiasi is an international project, currently supported by the following agencies: Météo-France, CNES, CNRS/INSU, NSF, NCAR, University of Wyoming, Purdue University, University of

Colorado, the Alfred Wegener Institute, the Met Office and ECMWF. Concordiasi also benefits from logistic or financial support of the operational polar agencies IPEV, PNRA, USAP and BAS, and from BSRN measurements at Concordia. Concordiasi is part of the THORPEX-IPY cluster within the International Polar Year effort. **Website: http://www.cnrm.meteo.fr/concordiasi/**

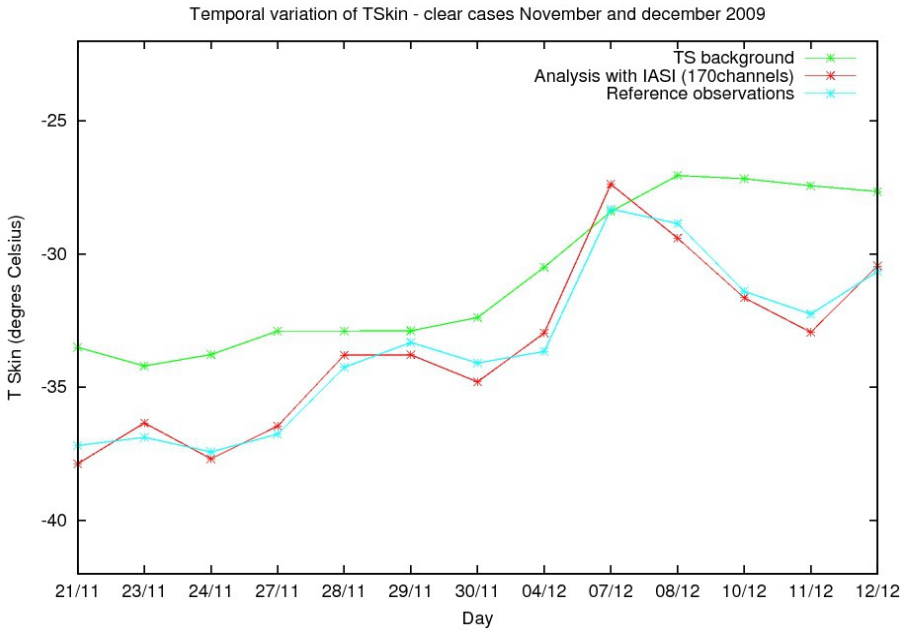

Figure 1 : Temporal series of surface temperature at Concordia. The model is drawn in red, with added IASI data in blue, in situ observations in black. In this figure, one can see a slight discrepancy between predictions from the model and data from in situ observations. Once the model is adjusted with IASI data, the combined estimations are much closer to those made in situ.

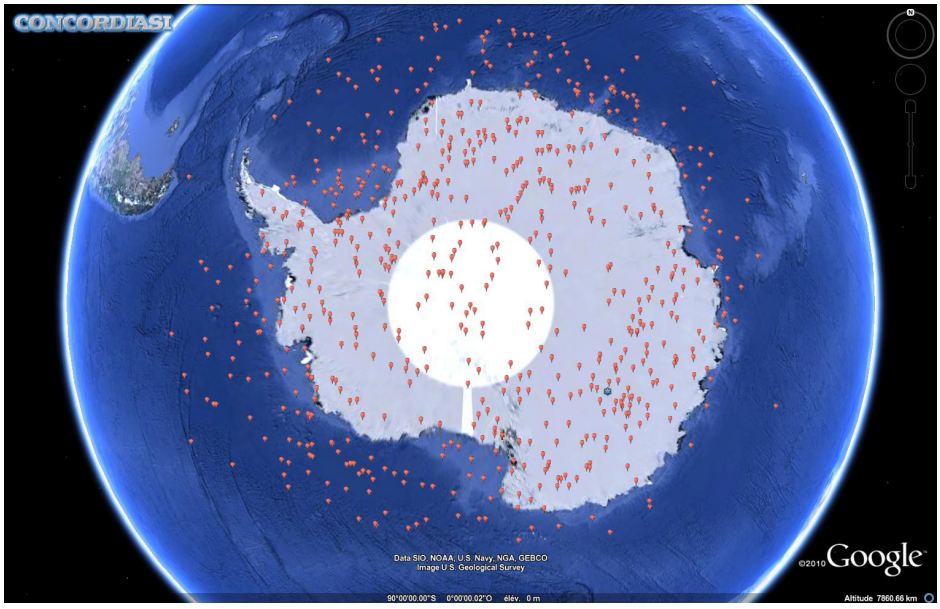

Figure 2: Location of the 275 dropsondes launched between the 23d of September and the 30th of November 2010.

References :

Rabier F., et al., The Concordiasi project in Antarctica, *Bull. Am. Meteorol. Soc.*, **91**, 69-86, doi: 10.1175/2009BAMS2764.1, 2010.

Development of an LETKF Nested System for a Cloud Resolving Model

Hiromu Seko, Tadashi Tsuyuki and Kazuo Saito
Meteorological Research Institute, Japan Meteorological Agency
E-mail; hseko@mri-jma.go.jp

1. Introduction

Assimilation methods for remote sensing data, such as radial wind of Doppler radars, have been developed at the Meteorological Research Institute (MRI) to improve the accuracy of the heavy rainfall forecast; the 3 dimensional data assimilation system for cloud resolving models and the mesoscale 4 dimensional data assimilation system and the Local Ensemble Transform Kalman Filter (LETKF) for mesoscale models. The results of these studies indicated that the horizontal convergence of low-level water vapor is essential to reproduce the heavy rainfalls. It was also reported that the large scale convergence (the environment of convections) of the first guess field should be modified by the ensemble forecast methods before the assimilation of cloud-scale data when the positional lag of the large scale convergence existed. In this report, an LETKF nested system, which modifies the large scale convergence by assimilation of conventional data and reproduces intense convection by assimilation of high resolution data, such as GPS PWV data, is explained and the preliminary results are also reported.

2. Outline of the LETKF nested system

The horizontal grid interval of the outer LETKF was 15 km, which is the same interval of the former studies (e.g. Seko et al. 2011). The domain was as large as 1900 km x 1900 km, which covers most of Japan. Surface and upper sounding data that were used in the operational mesoscale 4-dimensional assimilation system of the Japan Meteorological Agency were used as assimilation data of the outer model. These data were assimilated every hour in the 6-hour assimilation windows. The outer assimilation was performed from 00 UTC,1st September 2008 (5 days before the occurrence of an intense rainfall). The grid interval of the inner LETKF is set to 1.875 km to resolve individual convections. The initial and boundary conditions were produced by interpolating outputs of the outer LETKT. The domain of the inner LETKF is 300 km x 300 km that covers the local districts where the heavy rainfall occurred. The same data used for the outer LETKF were assimilated for the inner LETKF every 10 minutes with the assimilation windows of 1 hour. The analyzed fields of the outer LETKF were replaced every 6 hours by the analyzed fields produced by the inner LETKF (Figure 1).

3. Preliminary results of the nested LETKF system

On 5th September 2008, the intense rainfall, of which 1-hour rainfall exceeded 93 mm, was developed in the Osaka Plain, western Japan. This intense rainfall was chosen as the target event of assimilation experiments. Figure 2 shows the 1-hour rainfall distributions reproduced by the nested LETKF system at 06 UTC 5th. The outer LETKF reproduced the scatter rainfall regions on

the Pacific Ocean side of Japan. The rainfall region at Osaka was also reproduced in several ensemble members, though their rainfall intensities were much weaker than observations. In the inner LETKF, the predicted rainfall intensity exceeded 50 mm, in a few ensemble members. These rainfall amounts became larger than those of the outer LETKF, although they were still smaller than observations. This result indicates that the LETKF nested system has the potential to reproduce the intense rainfall. Other high-resolution data, such as radial winds of Doppler radar, are needed to reproduce the intense rainfall more properly.

References

H., Seko, T., Miyoshi, Y. Shoji, and K. Saito, Data assimilation experiments of precipitable water vapor using the LETKF system: intense rainfall event over Japan 28 July 2008, 2010, *Tellus A*, 63A (in printing).

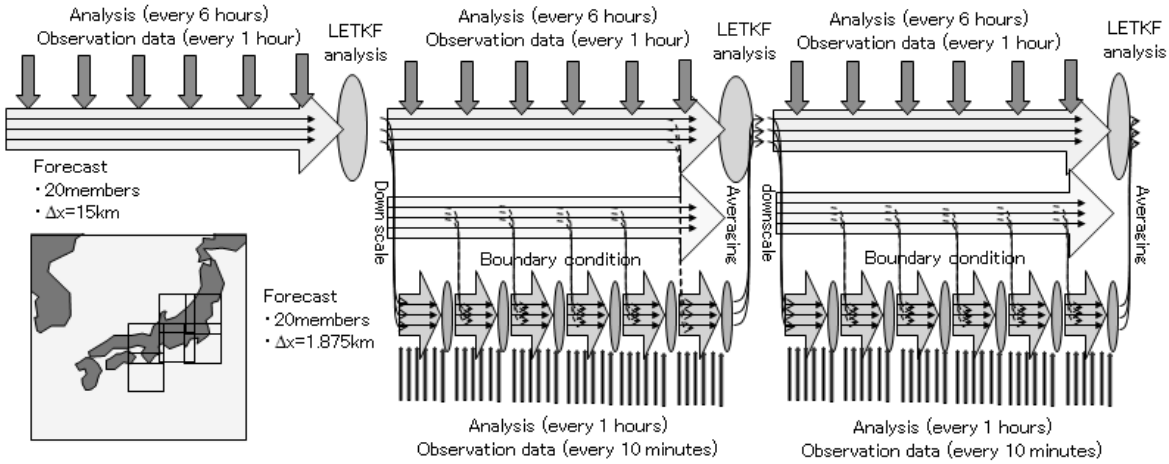

Fig. 1 Data flow chart of the LETKF nested system.

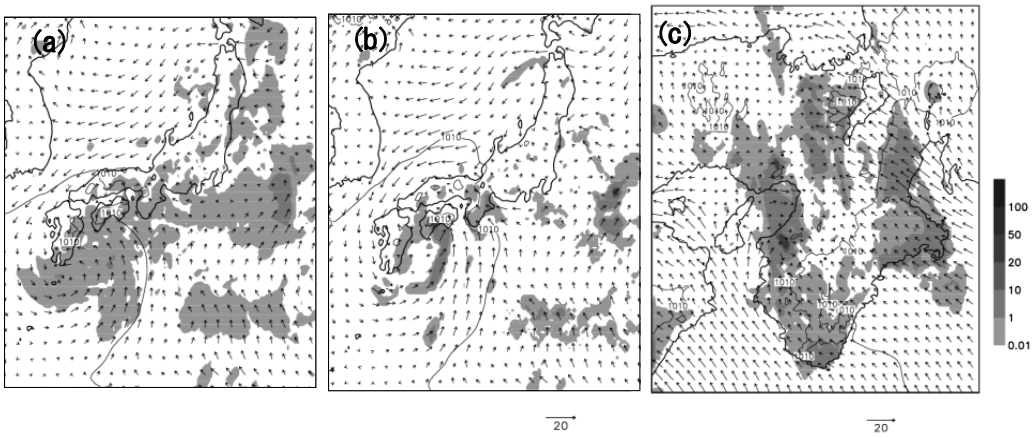

Fig. 2 Preliminary results of the LETKF nested system. (a) One hour rainfall distribution (shade) and horizontal wind (vector) of the ensemble mean of the outer LETKF at 06 UTC. (b) Same as (a) except for the member of #012. (c) Same as (b) except for the inner LETKF.

Data Assimilation Experiments of Vertical Gradient of Refractive Index Observed by Wind Profilers

Hiromu Seko[1], Kazuo Saito[1] and Toshitaka Tsuda[2]
[1]Meteorological Research Institute, Japan Meteorological Agency
[2]Research Institute for Sustainable Humanosphere, Kyoto University
E-mail; hseko@mri-jma.go.jp

1. Introduction

Water vapor is one of key factors for the improvement of the accuracy of rainfall forecasts. For instance, the impact of GPS-derived precipitable water vapor (PWV) data has been investigated by using the 4-dimensional data assimilation system (e.g. Seko et al., 2004). Besides GPS-derived PWV, the refractivity has information of water vapor. Furumoto et al. (2007) developed the method for estimation of the vertical profile of water vapor from vertical gradients of refractivity observed by the wind profiler by using the one-dimensional variational method. The Japan Meteorological Agency deploys 31 wind profilers (Wind Profiler Network and Data Acquisition System; WINDAS), in Japan. In this study, the vertical gradients of refractivity observed by WINDAS were assimilated by the 3-dimensional data assimilation system (JNoVA0) for non-hydrostatic model (NHM), and the impact of vertical gradients of refractivity on the forecast of intense rainfall is presented.

2. Thunderstorm observed at Osaka

At 06UTC 5th September 2008, an intense thunderstorm developed at the southern part of Osaka plain. Due to this intense thunderstorm, the 1-hour rainfall exceeding 90 mm was observed at the City of Sakai. This thunderstorm was generated by convergence of humid airflow that was enhanced by the thermo-dynamically-generated low-pressure area. So, this thunderstorm was chosen as the object for the data assimilation experiment.

3. Reproduction of the large-scale convergence and assimilation of Doppler data.

Because the first guess field given by the deterministic forecast could not reproduce the position of the convergence properly, the thunderstorm was not developed even in the forecast from the JNoVA0 analysis. Therefore, Local Ensemble Transform Kalman Filter (LETKF) was used to modify the large scale convergence. The analysis field among the ensemble members closest to the observed one was selected as the first guess field. The radial winds of Doppler Radar at Kansai and Osaka airports were assimilated by JNoVA0. Based on the statistics between the water vapor in the rainfall regions and updraft velocities, the atmosphere in the observed rainfall regions where the analyzed updraft velocities exceeded 0.15 m/s were assumed to be saturated. Besides this cloud scale water vapor modification, the mixing ratio of rain and snow estimated from the observed reflectivity with Z-R relation and analyzed temperature were placed at the grid points of NHM where it was observed in the domain of NHM. When these assimilation and modification were performed (Radial Wind (RW) case), the thunderstorm was reproduced (Fig. 2a).

4. Assimilation of the GPS data and the vertical gradient of the refractivity data

Besides the radial wind data and convective scale water vapor modification, the GPS-derived PWV and slant water vapor (SWV) were assimilated. When PWV or SWV were assimilated (PWV case and SWV case, respectively), the water vapor at the low levels was decreased, and then the thunderstorm was not reproduced (Fig. 2b). The comparison with the first guess and observed PWV shows that observed PWV/SWV around Osaka was smaller than first guess. Even if the PWV and SWV were smaller than the first guess, the

thunderstorm might be generated if the lower layer was more humid. To modify the vertical distribution of water vapor, the refractive index observed by WINDAS was assimilated as follows;

(1)The signs of vertical gradient of refractivity (M), which are not obtained by the wind profiler observation only, are determined by the 1d-Var. The cost-function of 1d-Var is composed of two parts; the difference from analyzed M and first guess M, and the difference of the analyzed M and the observed M. The combination of the sign of M whose cost-function is minimum is adopted (Fig. 1).
(2)The observed M with estimated signs is assimilated by JNoVA0.

When the vertical gradient of refractivity was added to assimilation data (PWV+M case), the rainfall region in the Kii Peninsula extended to Osaka Plain (Fig. 2c). Although the rainfall region was not reproduced perfectly, this result indicates that information of the refractive index may improve the rainfall forecast. The vertical cross-section of the analysis increment (difference between analyzed field and first guess field) indicates that the water vapor was increased below the height of 1 km in the region where the PWV was decreased in the PWV case (Fig. 3). This increment can be contributed to the northward extension of the rainfall region. The improvement was larger than that obtained by the assimilation of the slant water vapor data. When all signs were set to negative, the water vapor was unnaturally increased at the height of 5 km. This result indicates that proper estimation of the combination of signs of M is important.

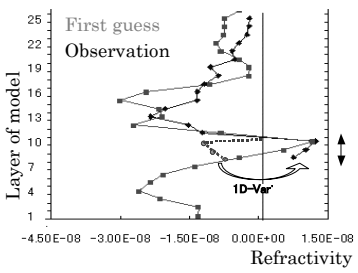

Fig.1: Schematic illustration for signs estimation of vertical gradient of refractivity (M).

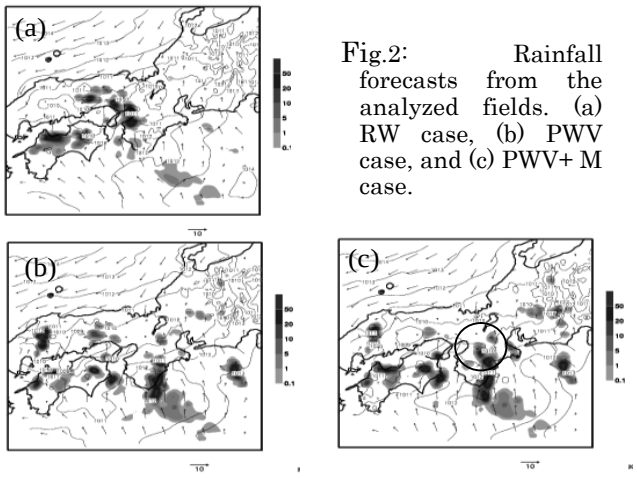

Fig.2: Rainfall forecasts from the analyzed fields. (a) RW case, (b) PWV case, and (c) PWV+ M case.

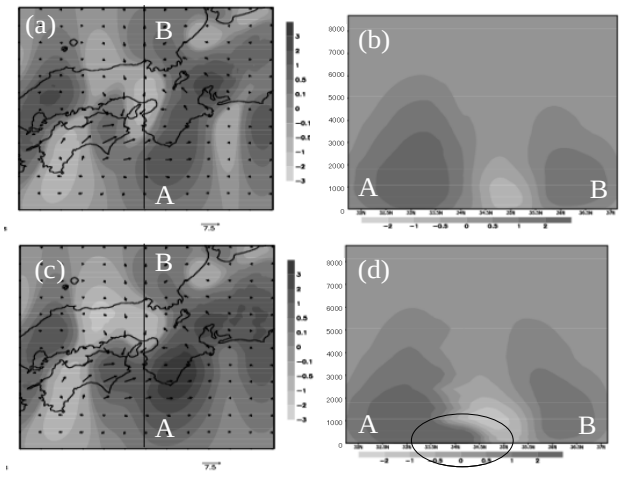

Fig. 3: Increment of water vapor at the lowest level. (a) PWV case and (c) PWV+M case. (b) and (d) Vertical cross-sections of the increment of water vapor along the lines in (a) and (c).

References

Furumoto, J., S. Imura, T. Tsuda, H. Seko, T. Tsuyuki, K. Saito, 2007: The Variational Assimilation Method for the Retrieval of Humidity Profiles with the Wind-Profiling Radar. *J. Atmos. Oceanic Technol.*, **24**, 1525–154

Seko, H. T. Kawabata, T. Tsuyuki, H. Nakamura, K. Koizumi and T. Iwabuchi, 2004: Impacts of GPS-derived Water Vapor and Radial Wind Measured by Doppler Radar on Numerical Prediction of Precipitation. *JMSJ*, **82**, 473-489.

Local Ensemble Transform Kalman Filter data assimilation: shallow water model tests

Anna Shlyaeva[1,2], Mikhail Tolstykh[3,1]
[1]Hydrometeorological Research Center of Russia, Moscow, Russia
[2]Bauman Moscow State Technical University, Moscow, Russia
[3]Institute of Numerical Mathematics, Russian Academy of Sciences, Moscow, Russia
email: shlyaeva@gmail.com

In this work, the local ensemble transform Kalman filter (LETKF) that is a local square root filter [2] suggested in [1] was implemented. The localization means that the analysis can be carried out independently at each grid point with the use of only local observations, which naturally decreases the problem size and reduces spurious correlations. One other distinctive feature of the LETKF is that it solves the problem in the ensemble space, using transformation from the physical to the ensemble space.

The LETKF assimilation scheme was tested with the shallow water model with forcing [3] on the sphere. The external forcing was chosen so that the mean state of the atmosphere on the specific pressure level was close to the NCEP/NCAR 2 reanalysis data for a given date (the approach similar to that of the tests with the barotropic vorticity model [4]). Model resolution is 1.5°×1.5°, the time step is equal to 45 minutes.

The assimilation scheme was tested in assimilation cycle. Pseudoobservations (wind components and geopotential) were generated from NCEP/NCAR 2 reanalysis in the randomly chosen grid points. We used NCEP/NCAR Reanalysis 2 data as first guesses at the first assimilation step. The localization function was piecewise linear, the influence distance being different for the wind components and for the geopotential.In the experimental set, the ensemble size was 40-60 members. The assimilation scheme is parallelized via MPI (each process calculates analysis for a chosen set of the latitude circles)

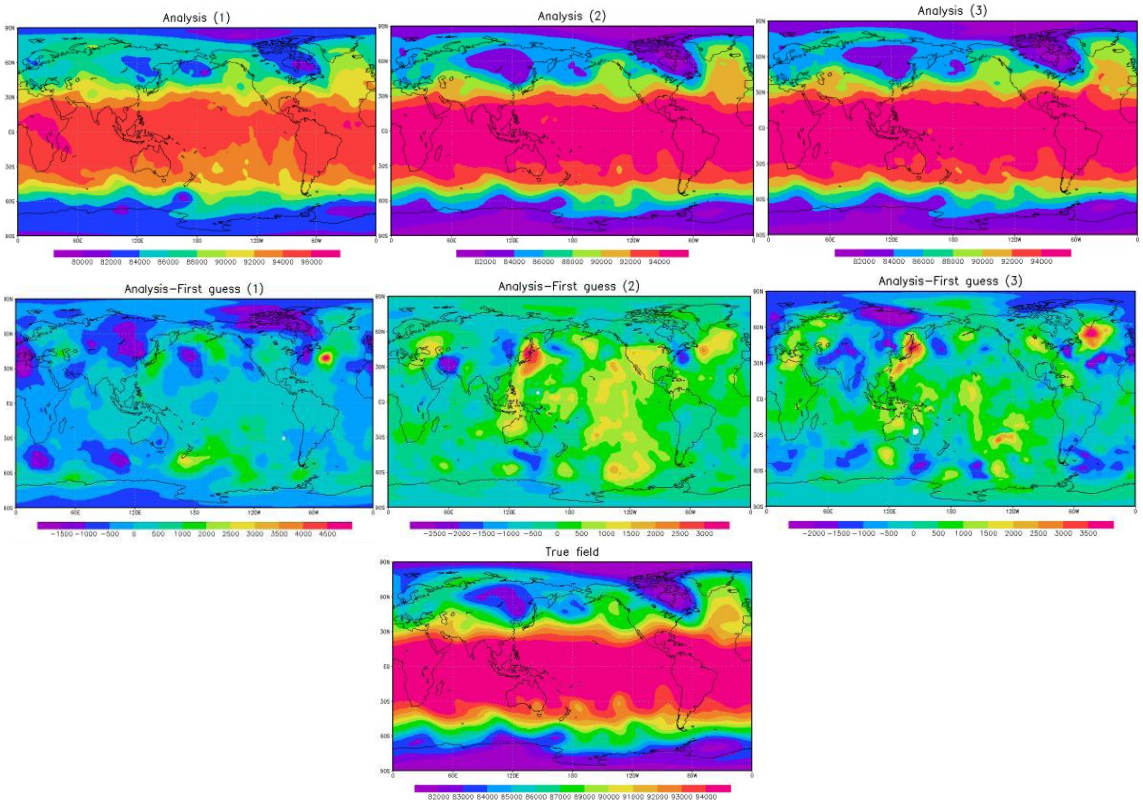

Figure 1 - Analysis (upper row), analysis increments (middle row) and true field (lower row) for the 250th assimilation step (left: inflation factor set to 1.1, middle: inflation factor set to 2, right: inflation factor set to 1.1, each ensemble member uses different forcings)

One of the most challenging points in the test suite was a serious underestimation of the analysis error covariance, which is a regular problem for the square root filter assimilation. Two possible solutions of the problem were devised. For the first one, we used a greater covariance inflation coefficient (equal to 2 or greater), artificially making the analysis error covariance greater by the factor of inflation. For the other one, we applied the model operator with different external forcing for different ensemble members (see Figure 1). Both approaches showed acceptable result, while using different external forcing seems to be more physical and is somewhat similar to the 'stochastic physics' approach [6].

The system proved to be stable for not less than 500 assimilation cycles.

The implemented LETKF assimilation scheme is now being tested with the 3D weather forecast model.

The work is partly supported by the RFBR grant 10-05-01066.

References:

1. Hunt, B.R., Kostelich, E.J. and Szunyogh, I., 2007: Efficient data assimilation for spatiotemporal chaos: a Local Ensemble Transform Kalman Filter. Physica D, 230, pp. 112-126.

2. Tippett, M.K, Anderson, J.L. and Bishop, C.H., 2003: Ensemble Square Root Filters. Mon. Wea. Rev., 131, pp. 1485-1490.

3. M.A. Tolstykh, 2002:Vorticity-divergence semi-Lagrangian shallow-water model on the sphere based on compact finite differences, J. Comput. Phys. v. 179, pp. 180-200.

4. Shlyaeva A.V., Tolstykh M.A., 2009: Local Ensemble Transform Kalman Filter for Semi-Lagrangian Barotropic Model of Atmosphere. The 5th WMO Symposium on Data Assimilation Extended Abstracts, 2009, Melbourne, p.216.1-216.5

5. Hong Li, E. Kalnay, T. Miyoshi, 2009: Simultaneous estimation of covariance inflation and observation errors within an ensemble Kalman filter, Quart. J. Roy. Met. Soc., v. 135, pp. 523-533.

6. Buizza, R., Milleer, M., Palmer, T.N., 2007: Stochastic representation of model uncertainties in the ECMWF ensemble prediction system. Quart. J. Roy. Met. Soc., v. 125, pp. 2887-2908.

Upgraded Usage of MODIS Polar Atmospheric Motion Vectors in the JMA Operational Global NWP System

Koji Yamashita

Numerical Prediction Division, Japan Meteorological Agency
e-mail: kobo.yamashita@met.kishou.go.jp

1. Introduction

MODIS is the Moderate Resolution Imaging Spectroradiometer on board the Terra and Aqua satellites, and MODIS polar Atmospheric Motion Vectors (AMVs) are estimated using MODIS sequential images over the polar regions. These AMVs have been produced by the Cooperative Institute for Meteorological Satellite Studies (CIMSS) since 2001, and have been assimilated in the Arctic since 27 May, 2004, with the Japan Meteorological Agency (JMA)'s operational global Numerical Weather Prediction (NWP) system (Kazumori and Nakamura 2004). CIMSS-AMVs in the Antarctic have also been used since 16 September, 2004. The data are acquired via anonymous FTP on CIMSS.

The National Oceanic and Atmospheric Administration (NOAA)/the National Environmental Satellite, Data, and Information Service (NESDIS) recently started producing MODIS polar AMVs (NESDIS-AMVs) on an operational basis. The data are broadcast internationally via the Global Telecommunication System (GTS). CIMSS also started producing new direct broadcast (DB) MODIS polar AMVs (CIMSS-DB-AMVs) to improve on the timeliness of CIMSS-AMVs. To enable the use of NESDIS-AMVs and CIMSS-DB-AMVs (the new AMVs) stably and instantly in operational global four-dimensional variational data assimilation (4D-VAR) on the NWP system (GSM-DA), we made several revisions to our quality control (QC) system. One-month observing-system experiments (OSEs) for the new AMVs were performed using GSM-DA with the revised QC system during January 2010 and August 2010.

2. Characteristics of the new AMV data

Figure 1 shows the data acquisition times for NESDIS-AMVs, CIMSS-DB-AMVs and CIMSS-AMVs for Terra in September 2008. The times for Terra CIMSS-DB-AMVs are much shorter than for the others, and those for NESDIS-AMVs are the same as those for CIMSS-AMVs. The new AMV data are expected to produce an increase in the volume of AMVs and to improve coverage in polar regions (Fig. 2).

The qualities of the new AMVs were evaluated statistically against the first guess of the GSM-DA. The standard deviation (STD) of the difference between the new AMVs and the first guess (O-B) is 3 – 4 m/s (not shown). The qualities of the new AMVs are as accurate as those of CIMSS-AMVs, but the spatial and time-error correlation distance of O-B in NESDIS-AMVs is longer than those of the other types (Fig. 2).

3. Revised QC for the new AMV data and OSEs

The major differences in QC between the operational method (CNTL) and the revised method (TEST) are shown in Table 1. We prioritize CIMSS-AMVs and CIMSS-DB-AMVs based on the results outlined in Section 2. Blacklisting in space was statistically decided by the mean error (ME) and STD of O-B in 2008. The criteria for O-B STD are 5 m/s for levels above 400 hPa, 4 m/s for levels from 400 to 700 hPa, and 2 m/s for levels below 700 hPa. An ME of below 2 m/s was adopted (Yamashita 2008). New IR AMVs, which showed statistically good quality for the 600 – 900 hPa level, were available for use.

OSEs were performed to evaluate the impact of the revised QC for the new AMVs using GSM-DA. Global 4D-VAR data assimilation cycles were run every six hours, and 216-hour forecasts were executed from 12 UTC using the operational global spectral model (JMAGSM), which is a hydrostatic spectral model with a horizontal resolution of 20 km (the resolution of the inner model for GSM-DA is 80 km) and 60 levels in the vertical direction with the top level at 0.1 hPa. The OSE periods were January and August of 2010.

4. OSE results

Figure 3 shows the forecast rate of improvement[1] with respect to RMSEs for forecasts covering periods from one to nine days in January 2010. Significant positive impacts are seen on three-day forecasts, especially in the Southern Hemisphere (SH), reaching up to 2 – 4% on average in January 2010. The RMSE of wind forecasts was reduced in the SH, especially below 300 hPa, against radiosonde observations in January 2010 (not shown). In August 2010, positive impacts were seen on typhoon track forecasts over 48 forecast hours (Figure 4), while the impact on the global forecast was almost neutral. In light of these OSE results, the revised QC system for polar AMVs was introduced into the JMA operational NWP system on 2 February, 2011.

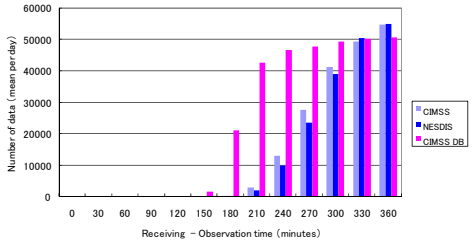

Figure 1. Data acquisition times for Terra NESDIS (blue), CIMSS DB (pink) and CIMSS operational (light blue) MODIS polar AMVs in September 2008

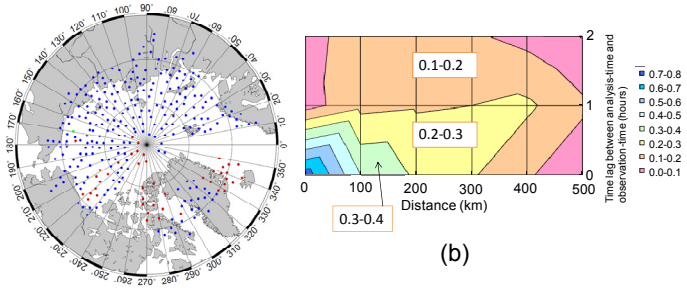

(a) (b)

Figure 2. (a) Polar AMVs used for the 400-hPa level in the North Pole region in JMA's NWP system at 00 UTC on August 29, 2010. The blue dots are for CIMSS-AMVs, the red dots are for CIMSS-DB-AMVs, and the green dots are for NESDIS-AMVs. (b) Spatial and time O-B error correlation for distance in Terra IR NESDIS-AMVs above 400 hPa in May 2009. The values show the O-B correlation coefficient.

Table 1: Major differences in QC between the operational method and the revised method

	Operational method (CNTL)	**Revised method (TEST)**
Data used	1. CIMSS- AMVs	1. CIMSS- AMVs 2. CIMSS-DB- AMVs 3. NESDIS- AMVs
Thinning	1. Thinning interval: 150 km 2. One AMV selected per box in the six-hour time window	1. Thinning interval: 150 km 2. Priority of CIMSS- AMVs and CIMSS-DB-AMVs 3. One AMV selected per box in the six-hour time window
Blacklisting in space *IR: infrared sensor *WV: water vapor sensor *CWV: clear sky WV	1. All AMVs over land below 400 hPa 2. All WV AMVs below 550 hPa over sea 3. All IR AMVs below 600 hPa over sea	1. IR* AMVs for NH above 300 hPa or below 900 hPa 2. WV* and CWV* AMVs for NH above 300 hPa or below 550 hPa 3. IR* and WV* AMVs for SH above 300 hPa or below 550 hPa 4. CWV* AMVs for SH above 350 hPa or below 550 hPa 5. All AMVs poleward of 88°N or 88°S
Observation error adjustment	Use	Not in use

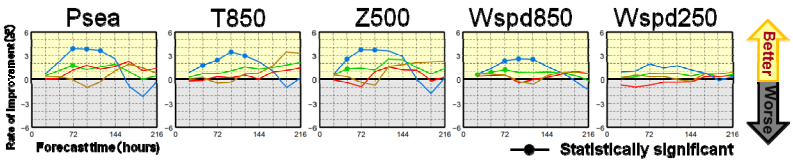

Figure 3. Forecast improvement rate with regard to RMSEs for 1 – 9-day forecasts in January 2010. The graph labeled Psea shows surface pressure, T850 shows 850-hPa temperatures, Z500 shows 500-hPa geopotential heights, Wspd850 shows 850-hPa wind speeds, and Wspd250 shows 250-hPa wind speeds. Positive values mean better scores. The green, brown, red and blue lines show the forecast improvement rate for the global, Northern Hemisphere (poleward of 20°N), tropical (20°S – 20°N) and Southern Hemisphere (poleward of 20°S) regions, respectively.

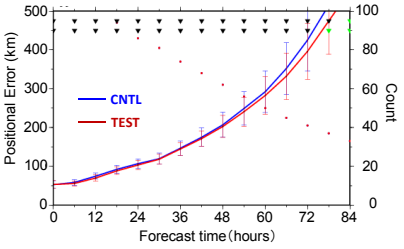

Figure 4. Average typhoon track forecast errors in August 2010. The red line is for TEST values, the blue line is for CNTL values, the red dots are sample data numbers, and the error bars represent a 95% confidence interval.

References

Kazumori, M. and Y. Nakamura, (2004): MODIS polar winds assimilation experiments at JMA, *Proceedings of 7th IWW*, Finland.

Yamashita, K., (2008): Upgraded Usage of Atmospheric Motion Vectors Geostationary Satellites in the Operational Global and Meso-Scale 4D-Var Assimilation System at JMA, *Proceedings of 9th IWW*, USA.

[1] $(RMSE_{CNTL} - RMSE_{TEST}) / RMSE_{CNTL}$

The Impacts of GPS Precipitable Water Assimilation in the JMA Global 4D-VAR Data Assimilation System

Koichi Yoshimoto
Numerical Prediction Division, Japan Meteorological Agency
1-3-4 Otemachi, Chiyoda-ku, Tokyo 100-8122, Japan
(E-mail: k-yoshimoto@met.kishou.go.jp)

1. Introduction

The International GNSS Service (IGS) operates a global network of ground-based GPS stations continuously for GPS satellite tracking, and provides GPS observation data via its FTP server. These data allow global estimation of ground-based GPS precipitable water (PW) data. We assessed the accuracy of global GPS-PW data and the related impact on JMA's global four-dimensional variational data assimilation system.

2. Outline of GPS-PW calculation and comparison with radiosonde-derived PW data

We used GIPSY-OASIS II software (GIPSY, Jet Propulsion Laboratory/NASA, Webb and Zemberg, 1993) for zenith tropospheric delay (ZTD) retrieval with the final ephemerides of IGS. Furthermore, in order to retrieve GPS-PW data derived from ZTD information, temperature and surface pressure data at IGS stations are required. Data from operational global analysis were used for this purpose.

In order to evaluate the accuracy of GPS-PW data, we compared them with PW values derived from radiosonde observation data (sonde-PW). In this comparison, we selected stations where the horizontal distance and the vertical height difference between GPS and the radiosonde station were less than 30 km and 200 m, respectively. Figure 1 shows scatter plots of GPS-PW values against sonde-PW data. The result shows good precision for GPS-PW, as indicated by the close correspondence to sonde-PW data.

3. Impact of GPS-PW on JMA's global data assimilation

We carried out observation system experiments for GPS-PW with a low-resolution (TL319L60) global data assimilation and forecasting system from August 1 – August 31, 2010. The forecasts were executed from each 12 UTC initial for the test run (with GPS-PW) and a control run (without GPS-PW). GPS-PW data satisfying the following conditions from the 192 stations shown in Figure 2 were used:

- The GPS-PW range was between 1 mm and 90 mm.
- The elevation difference between the model surface and the actual surface was less than 300 m.
- The PW difference between the first-guess value and the GPS-PW value was less than 10 mm.

In consideration of observation error correlation, the GPS-PW data were thinned using 100-km grid boxes. Only GPS-PW data observed at the analysis time were used. The PW correction of the elevation difference between the model surface and the actual surface was applied. The method is described in Ishikawa (2010).

Figure 3 shows average differences in the analyzed PW data between the control and the test (with GPS-PW). In the test, PW values are higher around IGS stations in the tropics. Figure 4 shows the improvement rate (%) of the test against the control for RMSE in the geopotential height forecast at 500 hPa. The result shows the positive impact of the GPS-PW assimilation.

References

[1] Webb, F. H. and J. F. Zumberge, 1993: An introduction to the GIPSY/OASIS-II. JPL Publ., D-11088.

[2] Ishikawa, Y., 2010: Data Assimilation of GPS Precipitable Water Vapor into the JMA Mesoscale Numerical Weather Prediction Model. CAS/JSC WGNE Res. Activ. Atmos. Oceanic Modell., 40, 01.13 – 01.14.

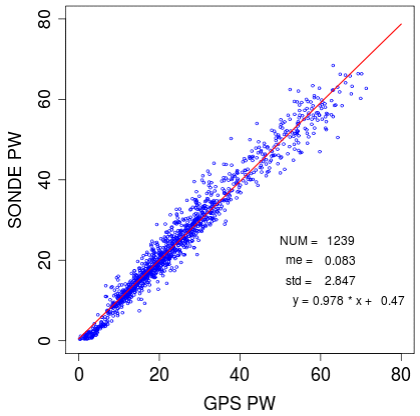

Figure 1: Scatter plots of GPS-PW data against sonde-PW values. The sampling period was from August 1 to August 31, 2010. The red line represents the linear regression derived from the scatter plots.

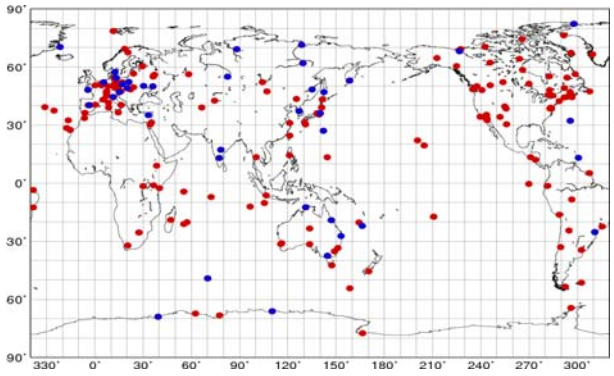

Figure 2: Location of IGS stations (192). The blue dots show the stations used for comparison with sonde-PW data.

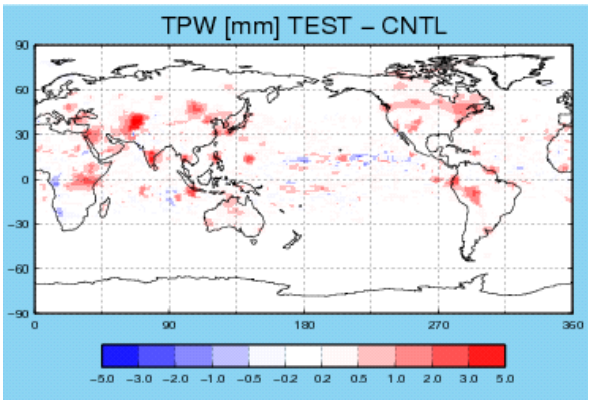

Figure 3: Average differences in analyzed values of PW between the control (without GPS-PW) and the test (with GPS-PW). The sampling period was from August 1 to August 31, 2010.

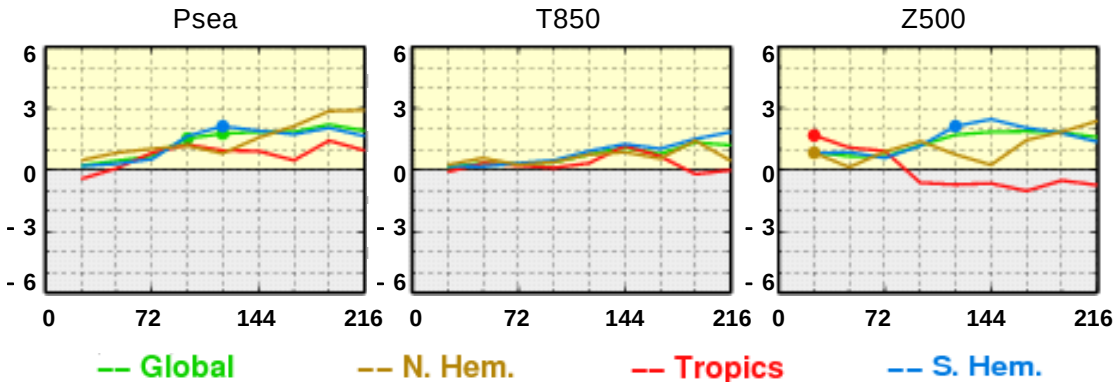

Figure 4: Improvement rate (%) in the RMSE of forecasting with GPS-PW against that without. The panels show surface pressure (left), T850 (middle) and Z500 (right). The horizontal axis represents the number of forecast hours. Lines appearing in the upper (yellow) area indicate a reduced RMSE. Dots on the score lines represent statistical significance.